AERODYNAMIC CHARACTERISTICS OF A HEMISPHERE AT HYPERSONIC SPEEDS

by

Edgar Brian Pritchard
III

Thesis submitted to the Graduate Faculty of the

Virginia Polytechnic Institute

in candidacy for the degree of

MASTER OF SCIENCE

in

Aeronautical Engineering

TABLE OF CONTENTS

LIST OF TABLES AND FIGURES

Page

Tables

Figures

I. INTRODUCTION

An investigation of guided missile performance will eventually lead to the consideration of flight at extremely large Mach numbers (of the order of 20 or larger). At these high Mach numbers the wing lift and drag may be satisfactorily obtained from two-dimensional gas dynamics since the opening angle of the Mach cone at the wing leading edge will be small. However, this is not the case for three-dimensional flow such as that over a body of revolution at angles of attack. Here body lift and drag constitute an appreciable portion of the total lift and drag of a winged missile at moderate angles of attack and high Mach numbers. Thus the determination of the aerodynamic lift and drag on axially symmetric bodies of revolution at hypersonic speeds is of increasing importance.

In this thesis an attempt has been made to analyze the lift and drag of a hemisphere in hypersonic flow through the application of Newton's corpuscular theory. The hemisphere has been chosen as the body type to be studied due to its increasing importance as a missile nose configuration.

The minimum drag shape is the Newtonian body. Truitt[4] points out that a cone frustum is a close approximation to the Newtonian body for small fineness ratios. Through the use of the calculus of variations the semivertex angle of the cone frustum was determined in terms of the semivertex angle of the cone inscribed

in the body under consideration. In this thesis the cone frustum having the same fineness ratio as the hemisphere is investigated and the results compared to those for the hemisphere.

The static and dynamic stability of the hemisphere, cone frustum and the cone inscribed in the hemisphere have been studied and compared.

At the high Mach numbers considered here the fluid pressure forces on the hemispherical body may be approximated in a relatively simple manner through the application of Newton's corpuscular theory. Newton's theory states that the fluid stream maintains its speed and direction unchanged until it comes into contact with a body. At the point of contact with a body the fluid stream gives up its component of momentum normal to the body surface and then moves along the surface of the body without loss of the tangential component of momentum. Those portions of the body surface which do not face, or "see" the flow, are considered to have no differential pressure forces acting on them. That is, the pressure coefficient is zero over these portions. It should be pointed out that, for a given Mach number and angle of attack, better results are obtained for a three-dimensional body than a two-dimensional body through the application of Newton's corpuscular theory.

The lift and drag coefficients have been obtained for a hemispherical nose configuration through the application of

Newton's impact theory for each angle of attack from zero to 90 degrees. Here, expressions for the lift and drag coefficients have been developed; first, neglecting the relieving effects of centrifugal forces acting on the fluid particles, i.e. considering only the Newtonian impact forces; and second, considering the interaction of the centrifugal and impact forces. The lift and drag coefficients obtained by neglecting the centrifugal force effects have been denoted as the Newtonian lift and drag coefficients. The expressions obtained yield only a first approximation to the true values. Therefore, in order to obtain what is felt to be a closer approximation to the true lift and drag coefficients for a hemisphere in hypersonic flow, the second expressions have been developed and are denoted as the Newtonian-plus-centrifugal lift and drag coefficients.

Centrifugal forces acting on a particle of air passing over a body surface arise due to the curvature of the surface. For example, consider a particle of air striking the hemisphere at some arbitrary point. According to Newtonian impact theory the particle instantly gives up its momentum normal to the surface at the point of impact. Actually, this is not the case since the particle is acted upon by centrifugal forces which to some extent counteract, or relieve, the impact forces. A method by which the centrifugal force effect can be determined has been studied by Ivey, Klunker and Bowen[1]. Here, a relation for the pressure

coefficient has been developed which includes these aforementioned centrifugal forces. From this relation the points on the body at which the pressure coefficient vanishes can be obtained thus defining the limits of integration for determining the aerodynamic parameters.

The aerodynamic characteristics and stability derivatives for cones have been studied quite thoroughly by Tobak and Wehrend[2]. Grimminger, Williams and Young[3] have also obtained solutions for the aerodynamic characteristics of a cone. Their results have been applied to the case of the cone frustum and the cone inscribed in the hemisphere. No attempt has been made to correct these expressions for centrifugal force effects since at small angles of attack there is negligible curvature of these two bodies in the flow direction. At higher angles of attack the path followed by a particle passing over the surface of either body would vary with angle of attack. This path could be elliptic, parabolic, hyperbolic, or circular in nature. But due to the difficulty in properly defining this path the effect of centrifugal forces would be exceedingly difficult to analyze.

In this investigation four stability parameters have been considered. They are:

1. C_{N_α} - The change in the normal force coefficient with respect to the angle of attack.

2. C_{N_q} - The change in the normal force coefficient with respect to the pitching velocity.

3. C_{m_α} - The change in the pitching moment coefficient with respect to the angle of attack.

4. C_{m_q} - The change in pitching moment coefficient with respect to the pitching velocity.

General expressions for these parameters are given in reference 2. These expressions have been applied to the three bodies under investigation in this thesis. Using these parameters the static and dynamic stability of each of these has been studied for the following physical conditions: a solid homogeneous body; a thin shell body without a base plate; and a thin shell body with a base plate. In addition, the effect of varying the cone frustum radii for a given fineness ratio has been investigated to ascertain the influence of this parameter on stability.

II. LIFT AND DRAG COEFFICIENTS FOR THE HEMISPHERE

The Newtonian Drag Coefficient

To obtain relations by which the Newtonian pressure forces acting on a hemisphere at angles of attack may be determined, consider the hemisphere of radius "a", shown in Figure 1. This figure shows the hemisphere at an angle of attack, α, where α is the angle between the free stream velocity vector, V_o, and the Y-axis. The angle θ denotes a local surface point. Figure 2 is a front view of the hemisphere where the shaded area is that portion of the hemisphere which does not "see" the flow. The angle ϕ denotes the length of a differential element of surface area on the "hidden" hemispherical area. Note that the surface area of that portion of the hemisphere which does not "see" the flow will be equal to the surface area of the "missing" area of the hemisphere. This "missing" area is the surface area from an angle of $90-\alpha$ degrees to an angle of 90 degrees in Figure 1 which, in the case of a sphere, "sees" the flow but which is nonexistent for the special case of a sphere, namely the hemisphere.

It shall now be the purpose of the present investigation to determine a relation for the Newtonian drag coefficient for the hemisphere at angle of attack. It is well known that a sphere under the application of Newton's corpuscular theory yields a drag coefficient of one. Thus the Newtonian drag coefficient for the

hemisphere at angle of attack may be obtained by subtracting the drag coefficient acting on the ''missing'' area from the drag coefficient for the hemisphere at zero degrees angle of attack, which corresponds to the drag coefficient for a sphere.

Therefore, the Newtonian drag coefficient may be written in the general form:

$$C_{D_N} = 1 - C_{D_M} \quad . \tag{1}$$

Now, in order to obtain the term C_{D_M} in equation (1) consider a differential element of surface area, ds, at an arbitrary point, denoted by the angle θ, on the hemisphere surface between values of θ of $\frac{\pi}{2} - \alpha$ and $\frac{\pi}{2}$. The differential element has a width, $ad\theta$, and a length, 2ϕ a sin θ. The component of this area normal to the drag direction is,

$$ds_D = 2\phi\, a^2 \sin\theta \cos\theta\, d\theta \quad . \tag{2}$$

The drag force acting on the differential surface element is then,

$$dD = (P_L - P_o)(2\phi\, a^2 \sin\theta \cos\theta)\, d\theta \quad . \tag{3}$$

Integrating this expression between the limits $\frac{\pi}{2} - \alpha$ and $\frac{\pi}{2}$ yields the total drag force acting on the ''missing'' areas. That is,

$$D = \int_{\frac{\pi}{2} - \alpha}^{\frac{\pi}{2}} (P_L - P_o)(2\phi\, a^2 \sin\theta \cos\theta)\, d\theta \quad . \tag{4}$$

Defining the drag coefficient as

$$C_D = \frac{D}{\pi\, q\, a^2} \tag{5}$$

the drag coefficient for the ''missing'' hemispherical area may be written in the form

$$C_{D_M} = \int_{\frac{\pi}{2} - \alpha}^{\frac{\pi}{2}} \frac{(P_L - P_o)}{\pi\ q} (2\phi \sin\theta \cos\theta)\, d\theta \tag{6}$$

where the term $\frac{P_L - P_o}{q}$ is the pressure coefficient acting on the hemisphere. However, from Newton's impact theory, the pressure coefficient may be written for the present coordinate system as:

$$C_p = 2 \cos^2\theta \quad . \tag{7}$$

Therefore, equation (6) becomes, upon substitution of equation (7),

$$C_{D_M} = \frac{4}{\pi} \int_{\frac{\pi}{2} - \alpha}^{\frac{\pi}{2}} \phi \sin\theta \cos^3\theta\, d\theta \quad . \tag{8}$$

The angle ϕ may now be obtained in terms of the angles θ and $\frac{\pi}{2} - \alpha$ from consideration of Figure 2. From this figure it may be seen that:

$$\cos\phi = \frac{z}{s} \tag{9}$$

where:

$$z = a \tan\left(\frac{\pi}{2} - \alpha\right)$$
$$s = a \tan\theta \tag{10}$$

From equations (9) and (10) the angle ϕ may be written as:

$$\phi = \cos^{-1}\left[\cot\theta \tan\left(\frac{\pi}{2} - \alpha\right)\right] \quad . \qquad (11)$$

Substitution of equation (11) in equation (8) yields the drag coefficient for the "missing" hemispherical area in its final form. That is:

$$C_{D_M} = \frac{4}{\pi} \int_{\frac{\pi}{2} - \alpha}^{\frac{\pi}{2}} \cos^3\theta \sin\theta \cos^{-1}\left[\cot\theta \tan\left(\frac{\pi}{2} - \alpha\right)\right] d\theta \qquad (12)$$

Now, from the previous discussion of the total drag coefficient for the hemisphere at angle of attack, the substitution of equation (12) in equation (1) will yield the Newtonian drag coefficient for the hemisphere. That is,

$$C_{D_N} = 1 - \frac{4}{\pi} \int_{\frac{\pi}{2} - \alpha}^{\frac{\pi}{2}} \cos^3\theta \sin\theta \cos^{-1}\left[\cot\theta \tan\left(\frac{\pi}{2} - \alpha\right)\right] d\theta \quad . \qquad (13)$$

Equation (13) may not be integrated exactly; therefore, a graphical integration process was used in the solution of this equation for the drag coefficient. This process is presented briefly below.

For the angle of attack under consideration numerous values of θ were chosen between the limits, $\frac{\pi}{2} - \alpha$ to $\frac{\pi}{2}$. Equation (12) was then solved for values of C_{D_M} at local points on the surface. These local values of C_{D_M} were then plotted versus θ and the area under this curve was the total C_{D_M}

for the angle of attack under consideration.

Although this method of integration is most laborious, it is felt that greater accuracy may be obtained by the present method than by other available methods.

The Newtonian drag coefficient is presented graphically in Figure 6 as a function of angle of attack. Also, the Newtonian drag coefficient is presented in Table 1 for each angle of attack from zero to 90 degrees.

The Newtonian Lift Coefficient.

Newton's corpuscular theory predicts that the lift coefficient will be zero for a sphere. This is apparent from consideration of the pressure forces acting on a sphere. Since the lift coefficient for the hemisphere is zero at zero degrees angle of attack, the Newtonian lift coefficient may be determined from consideration of the pressure forces acting on the "missing" hemispherical area in the lift direction. Thus the Newtonian lift coefficient may be written in the form,

$$C_{L_N} = - C_{L_M} \quad , \tag{14}$$

where the negative sign enters the equation due to the fact that the actual lift forces acting on the hemisphere will be in the opposite direction from the lift forces acting on the "missing" area.

Again considering the previously defined differential element of area where it is now desired to use the component of differential area normal to the lift direction,

$$ds_L = 2\, a^2 \sin^2 \theta \sin \phi \, d\theta \quad . \tag{15}$$

The lift force acting on this element of area is,

$$dL = (P_L - P_o)\,(2\, a^2 \sin^2 \theta \sin \phi\,)\, d\theta \quad , \tag{16}$$

and the total lift force acting on the ''missing'' area may be obtained by the integration of equation (16) over the interval of θ from $\frac{\pi}{2} - \alpha$ to $\frac{\pi}{2}$. Thus,

$$L = \int_{\frac{\pi}{2} - \alpha}^{\frac{\pi}{2}} (P_L - P_o)(2\, a^2 \sin^2 \theta \sin \phi)\, d\theta \quad . \tag{17}$$

Defining the lift coefficient in a manner similar to the drag coefficient,

$$C_L = \frac{L}{\pi\, q\, a^2} \tag{18}$$

the lift coefficient acting on the ''missing'' area may be written as:

$$C_{L_M} = \int_{\frac{\pi}{2} - \alpha}^{\frac{\pi}{2}} \frac{(P_L - P_o)}{\pi\, q} \,(2 \sin^2 \theta \sin \phi)\, d\theta \quad . \tag{19}$$

Equation (19) becomes, upon substitution of equation (7), the Newtonian pressure coefficient:

$$C_{L_M} = \frac{4}{\pi} \int_{\frac{\pi}{2} - \alpha}^{\frac{\pi}{2}} \cos^2 \theta \sin^2 \theta \sin \phi \, d\theta \quad . \tag{20}$$

The quantity sin ϕ may be obtained in terms of the angles θ and $\frac{\pi}{2} - \alpha$. It has been shown previously that,

$$\cos \phi = \frac{\tan (\frac{\pi}{2} - \alpha)}{\tan \theta} \quad . \tag{21}$$

Thus the side opposite the angle ϕ is,

$$Y = \sqrt{\tan^2\theta - \tan^2 (\tfrac{\pi}{2} - \alpha)} \tag{22}$$

and therefore the sine of the angle ϕ may be written as:

$$\sin \phi = \frac{\sqrt{\tan^2 \theta - \tan^2 (\frac{\pi}{2} - \alpha)}}{\tan \theta} \tag{23}$$

Substituting equation (23) in equation (20) and simplifying the lift coefficient becomes:

$$C_{L_M} = \frac{4}{\pi} \int_{\frac{\pi}{2} - \alpha}^{\frac{\pi}{2}} \cos^2 \theta \sin \theta \sqrt{1 - \left[1 + \tan^2 (\tfrac{\pi}{2} - \alpha)\right] \cos^2 \theta} \, d\theta \tag{24}$$

Equation (24) may be integrated by parts with the aid of a transformation of variables to obtain, before the substitution of the limits:

$$C_{L_M} = \frac{4}{3\pi K}\left[\cos\theta\,(1 - K\cos^2\theta)^{3/2} - \frac{\cos\theta}{8}\,(5 - 2K\cos^2\theta)\sqrt{1 - K\cos^2\theta}\right.$$

$$\left. - \frac{3}{8\sqrt{K}}\,\sin^{-1}\left(\sqrt{K}\cos\theta\right)\right]_{\frac{\pi}{2} - \alpha}^{\frac{\pi}{2}} \qquad (25)$$

where: $K = 1 + \tan^2\left(\frac{\pi}{2} - \alpha\right)$

This equation reduces (upon substitution of the limits) to:

$$C_{L_M} \doteq 1/4\,\cos^3\left(\frac{\pi}{2} - \alpha\right) \qquad (26)$$

The Newtonian lift coefficient acting on the hemisphere at angle of attack may now be obtained from equations (14) and (26),

$$C_{L_N} = -\,1/4\,\cos^3\left(\frac{\pi}{2} - \alpha\right) \qquad (27)$$

Note that in equation (27) the Newtonian lift coefficient will be negative for positive angles of attack as is to be expected. Equation (27) is presented graphically as a function of angle of attack in Figure 7 and is also presented in Table 1.

At this point the lift and drag coefficients have been obtained for the restrictions of pure Newtonian flow. However, it is well known that centrifugal forces act on the air particles passing over a curved surface. These centrifugal forces cause the air particles to leave the surface of the hemisphere earlier than predicted by Newtonian theory. Therefore, it has also been the purpose of this thesis to determine a centrifugal force correction

to the previously defined Newtonian lift and drag coefficients to obtain a closer approximation to the true values of lift and drag coefficient for the hemisphere at angles of attack.

Newtonian-Plus-Centrifugal Drag Coefficient

Ivey, Klunker, and Bowen[1] have developed a relation for the pressure coefficient which includes the effects of centrifugal forces. The principal assumption involved in the development of this relation is that the shock wave lies on the boundary layer and has the same radius of curvature at any point as the body at the corresponding point on its surface. The effect of this assumption is to overpredict the relieving effect of the centrifugal forces.

The pressure coefficient[1] may be written in terms of the present coordinate system as:

$$C_p = 2 \cos^2 \theta - 2/3 \sin^2 \theta \qquad (28)$$

Equation (28) may now be used to determine the Newtonian-plus-centrifugal lift and drag coefficients.

Recalling the previous definition of the drag coefficient acting on the "missing" area,

$$C_{D_M} = \frac{2}{\pi} \int C_p \phi \sin \theta \cos \theta \, d\theta \quad , \qquad (29)$$

and applying the general trigonometric transformation to equation (28) to obtain the pressure coefficient as a function of cos θ only,

then

$$C_p = 2/3\ (4\cos^2\theta - 1)\ , \tag{30}$$

so that the ''missing'' area drag coefficient becomes, upon substitution of equation (30) into equation (29),

$$C_{D_M} = \frac{4}{3\pi} \int (4\cos^2\theta - 1)\ \phi \sin\theta \cos\theta\, d\theta\ , \tag{31}$$

which may be separated into two integrals

$$C_{D_M} = \frac{16}{3\pi} \int \phi \cos^3\theta \sin\theta\, d\theta - \frac{4}{3\pi} \int \phi \sin\theta \cos\theta\, d\theta\ . \tag{32}$$

Now define the two components of this equation as:

$$C_{D_{M_1}} = \frac{16}{3\pi} \int \phi \cos^3\theta \sin\theta\, d\theta \tag{33}$$

and

$$C_{D_{M_2}} = \frac{4}{3\pi} \int \phi \sin\theta \cos\theta\, d\theta \tag{34}$$

Note that equation (33) is of the same form as the previously obtained Newtonian drag coefficient on the ''missing'' area. Therefore, a similar graphical integration process must be applied to equation (33) to obtain a solution to this equation.

At this point the limits of integration must be determined. Since the Newtonian-plus-centrifugal drag coefficient will be determined in the same manner as the Newtonian drag coefficient; that is, the drag coefficient acting on the ''missing'' area will be subtracted from the drag coefficient for the hemisphere at zero

angle of attack; the limits will be those of the "missing" area. The lower limit will again be $\frac{\pi}{2} - \alpha$. However, the upper limit will be the angle, θ_i, at which the pressure coefficient first goes to zero on the hemispherical nose. This angle may be obtained by setting equation (28) equal to zero and solving for θ_i. This value of θ will be the upper limit since from the point on the hemispherical surface defined by the angle θ_i to an angle of 90 degrees the pressure coefficient (and hence the drag coefficient) will be zero. Or,

$$C_{p_i} = 0 = 2 \cos^2 \theta_i - 2/3 \sin^2 \theta_i \qquad (35)$$

which may be readily solved to yield a value of θ_i of 60 degrees.

Thus the limits of integration of equations (33) and (34) will be from $\frac{\pi}{2} - \alpha$ to $\frac{\pi}{3}$. Note that for an angle of attack equal to or less than 30 degrees the "missing" area will be a portion of the hemisphere over which the pressure coefficient is zero (see Figure 3) and hence the Newtonian-plus-centrifugal drag coefficient will be a constant for this range of angle of attack. Thus equations (33) and (34) become, upon substitution of equation (11) for the term ϕ,

$$C_{D_{M_1}} = \frac{16}{3\pi} \int_{\frac{\pi}{2} - \alpha}^{\frac{\pi}{3}} \cos^3 \theta \sin \theta \cos^{-1}\left[\cot \theta \tan \left(\frac{\pi}{2} - \alpha\right)\right] d\theta \qquad (36)$$

and

$$C_{D_{M_2}} = \frac{4}{3\pi} \int_{\frac{\pi}{2} - \alpha}^{\frac{\pi}{3}} \sin\theta \cos\theta \cos^{-1}\left[\cot\theta \tan\left(\frac{\pi}{2} - \alpha\right)\right] d\theta \qquad (37)$$

Equation (36) must be solved by the graphical integration process previously discussed. The integration of equation (37), by the method of integration by parts and a transformation of variable, yields upon substitution of the limits:

$$C_{D_{M_2}} = \frac{4}{3\pi}\left\{ \frac{3}{8} \cos^{-1}\left[\frac{\tan\left(\frac{\pi}{2} - \alpha\right)}{\sqrt{3}} \right] + \right.$$

$$\left. \frac{\tan\left(\frac{\pi}{2} - \alpha\right)}{2\sqrt{K}} \left[\left(\sin^{-1} \frac{\sqrt{K}}{2}\right) - \frac{\pi}{2} \right] \right\} \qquad (38)$$

The value of the Newtonian-plus-centrifugal drag coefficient for zero degrees angle of attack must now be determined. This value can be obtained from the following equation,

$$C_{D_{\alpha = 0}} = \frac{4}{3} \int_{0}^{\frac{\pi}{3}} (4\cos^2\theta - 1) \sin\theta \cos\theta \, d\theta \quad , \qquad (39)$$

where:

$$\phi = \pi, \quad \text{for} \quad \alpha = 0$$

The integration of equation (39) yields a value for $C_{D_{\alpha = 0}}$ of

$$C_{D_{\alpha = 0}} = 0.75 \quad . \qquad (40)$$

Therefore the Newtonian-plus centrifugal drag coefficient is:

$$C_{D_{N + C}} = 0.75 - C_{D_M} \quad , \qquad (41)$$

which, upon substitution of equations (36) and (38) for the second term of this equation, becomes

$$C_{D_{N+C}} = 0.75 - \frac{16}{3\pi} \int_{\frac{\pi}{2} - \alpha}^{\frac{\pi}{2}} \cos^3 \theta \sin \theta \cos^{-1} \left[\cot \theta \tan \left(\frac{\pi}{2} - \alpha \right) \right] d\theta$$

$$+ \frac{4}{3\pi} \left\{ \frac{3}{8} \cos^{-1} \left[\frac{\tan \left(\frac{\pi}{2} - \alpha \right)}{\sqrt{3}} \right] + \frac{\tan \left(\frac{\pi}{2} - \alpha \right)}{2\sqrt{a}} \left[\sin^{-1} \frac{\sqrt{K}}{2} - \frac{\pi}{2} \right] \right\}. \tag{42}$$

where: $a = \tan^2 \left(\frac{\pi}{2} - \alpha \right)$ and $K = 1 + a$.

Note that for $\alpha = 30$ degrees the Newtonian-plus-centrifugal drag coefficient will have a value of

$$C_{D_{N+C}} = 0.75 \tag{43}$$

Equation (42) has been plotted as a function of angle of attack in Figure 6. Equation (13), the Newtonian drag coefficient, is also included in this figure. The results of equation (42) and equation (13), as presented in Figure 6, will be discussed and compared in a later section of this thesis. The quantity $C_{D_{N+C}}$ has also been presented in Table 1 for each angle of attack from zero to 90 degrees.

Newtonian-Plus-Centrifugal Lift Coefficient

Making use of the previously defined pressure coefficient, which includes the relieving effect of the centrifugal forces, the Newtonian-plus-centrifugal lift coefficient will now be

obtained. Recall that the lift coefficient for the ''missing'' area of the hemisphere at angles of attack has been defined as

$$C_{L_M} = \frac{2}{\pi} \int C_p \sin^2 \theta \sin \phi \, d\theta \quad . \tag{44}$$

Substituting equation (28) for the pressure coefficient and making use of the previously determined expression for the sine of the angle ϕ, equation (44) becomes:

$$C_{L_M} = \frac{4}{3\pi} \int (4 \cos^2 \theta - 1) \sin \theta \sqrt{1 - K \cos^2 \theta} \, d\theta \quad . \tag{45}$$

Recalling that the limits of integration for the lift coefficient on the ''missing'' area are from $\frac{\pi}{2} - \alpha$ to $\frac{\pi}{3}$, and changing the sign of equation (45) to obtain the correct sign for the lift coefficient acting on the hemisphere, equation (45) becomes:

$$C_{L_{N+C}} = \frac{-4}{3\pi} \int_{\frac{\pi}{2} - \alpha}^{\frac{\pi}{3}} (4 \cos^2 \theta - 1) \sin \theta \sqrt{1 - K \cos^2 \theta} \, d\theta \quad . \tag{46}$$

Equation (46) may be integrated directly to obtain a closed form solution for the Newtonian-plus-centrifugal lift coefficient for the hemisphere at angle of attack. Such an integration gives:

$$C_{L_{N+C}} = \frac{-4}{3\pi} \left\{ \frac{1}{2K} \left(1 - \frac{K}{4}\right)^{3/2} + \frac{1}{4} \left(1 - \frac{1}{K}\right) \sqrt{1 - \frac{K}{4}} \right.$$

$$\left. + \frac{1}{2\sqrt{K}} \left[1 - \frac{1}{K} \sin^{-1} \frac{\sqrt{K}}{2} - \frac{\pi}{4\sqrt{K}} \left(1 - \frac{1}{K}\right) \right] \right\} \tag{47}$$

where:

$$K = 1 + \tan^2 \left(\frac{\pi}{2} - \alpha\right) \quad .$$

The Newtonian and Newtonian-plus-centrifugal lift and drag coefficients have now been obtained for the hemisphere at angle of attack. Equations (25) and (47) are compared for the range of angles of attack in Figure 7 and Table 1.

It is felt that in order to obtain a better picture of the hemisphere, aerodynamically, it should be compared with its inscribed cone and also the minimum-drag cone frustum of the same fineness ratio. In the following sections the aerodynamic characteristics of the inscribed cone and minimum-drag cone frustum are determined.

Inscribed Cone ($\delta = 45^\circ$)

From geometrical considerations the inscribed cone will necessarily have a semivertex angle, δ, of 45 degrees. Two specific physical cases must be considered, when determining the force coefficients acting on these bodies, in accord with the assumptions of Newton's impact theory. These are:

1. Angles of attack less than or equal to the semivertex angle of the cone.
2. Angles of attack greater than the semivertex angle of the cone.

For case 1, the entire surface of the cone "sees" the flow and

the term ω_u, defined in Figure 4, takes on the value of $\frac{\pi}{2}$. For the second case a portion of the cone surface does not "see" the flow. Here, the term ω_u is a function of the semivertex angle of the cone and the angle of attack.

Grimminger, Williams and Young[3] have developed general expressions by which the normal and chordwise force coefficients for a cone may be defined for each of the above cases. These expressions may be written, in terms of the coordinate system used here, as:

Case 1: $\alpha \leq \delta$

$$C_N = \sin 2\alpha \sin \delta \cos \delta \qquad (48)$$

and $$C_C = \tan \delta \; 2 \sin^2 \delta + \sin^2 \alpha \, (1 - 3 \sin^2 \delta)$$

where $\omega_u = \frac{\pi}{2}$.

Case 2: $\alpha > \delta$

$$C_N = \cos^2 \delta \sin 2\alpha \left(\frac{\omega_u + \frac{\pi}{2}}{\pi} \right) + \\ + \frac{1}{3\pi} \cos \omega_u \, (\tan \delta \cot \alpha + 2 \cot \delta \tan \alpha)$$

and $$C_C = \left(\frac{\omega_u + \frac{\pi}{2}}{\pi} \right) 2 \sin^2 \delta + \sin^2 \alpha \, (1 - 3 \sin^2 \delta) \\ + \frac{3}{4\pi} \cos \omega_u \sin 2\delta \sin 2\alpha \; . \qquad (49)$$

where:

$$\omega_u = \sin^{-1} \left(\frac{\tan \delta}{\tan \alpha} \right)$$

The Newtonian lift and drag coefficients are obtained from equations (48) and (49) by simply transforming the normal and chordwise force coefficients into the lift and drag coefficients. The transformations lead immediately to the relations

$$C_L = C_N \cos \alpha - C_C \sin \alpha$$

and

$$C_D = C_N \sin \alpha + C_C \cos \alpha \quad . \tag{50}$$

For the specific cone considered here (δ = 45 degrees) equations (48) and (49) are substituted into equations (50). After simplification, the lift and drag coefficients (for the cone) become:

Case 1: $\alpha \leq 45^\circ$

$$C_L = -\frac{\sin^3 \alpha}{2}$$

and

$$C_D = \cos \alpha \left(1 + \frac{\sin^2 \alpha}{2}\right) \tag{51}$$

Case 2: $\alpha > 45^\circ$

$$C_L = \frac{\cos \alpha \sqrt{1 - \cot^2 \alpha}}{6\pi} - \frac{\sin^3 \alpha}{2\pi}\left(\sin^{-1}(\cot \alpha) + \frac{\pi}{2}\right)$$

and

$$C_D = \frac{\cos \alpha}{\pi}\left(1 + \frac{\sin^2 \alpha}{2}\right)\left[\sin^{-1}(\cot \alpha) + \frac{\pi}{2}\right] + \frac{\sin \alpha}{6\pi}\sqrt{1 - \cot^2 \alpha}\,(11 - 7 \sin^2 \alpha) \quad . \tag{52}$$

The Newtonian lift and drag coefficients, as obtained from equations (51) and (52) are presented as a function of angle of attack in Figures 8 and 9.

It is now desirable to define the minimum-drag cone frustum for a fineness ratio of one-half in order to compare its aerodynamic characteristics with those of the hemisphere and the inscribed cone. This will be done in the next section.

Minimum-Drag Cone Frustum

Truitt[4] pointed out that the minimum-drag or Newtonian body, for Mach numbers very much greater than unity and for small fineness ratio, may be approximated by a cone frustum. In this thesis the minimum-drag cone frustum is determined for a fineness ratio of one-half, corresponding to that of the hemisphere. It has been shown[4], by means of the minimizing process of the calculus of variations, that the semivertex angle of the minimum-drag cone frustum is related to the semivertex angle of the cone inscribed in the body whose drag coefficient is being minimized. These angles are related by the expression,

$$\tan 2\delta_{C.F.} = 2 \tan \delta_C \qquad (53)$$

where: $\delta_{C.F.}$ = semivertex angle of the minimum-drag cone frustum. (See Figure 5a).

and δ_C = semivertex angle of the inscribed cone.

For the present case, the inscribed cone has a semivertex angle of 45 degrees. Thus the semivertex angle of the minimum-drag cone frustum is found to be

$$\delta_{C.F.} = 31.7 \text{ degrees} .$$

The radius of the forward face of the cone frustum, R_o, is readily determined to be:

$$R_o = 0.3824 \ R_B \ ,$$

since:

$$\tan \delta_{C.F.} = \frac{R_B - R_o}{R_B} \ .$$

Having now determined the pertinent dimensions of the minimum-drag cone frustum, the Newtonian lift and drag coefficients may be obtained as a function of angle of attack. This is carried out in the next section.

Force Coefficients for the Cone Frustum

The Newtonian lift and drag coefficients for the cone frustum may be obtained in the same manner as for the cone. The general solutions for the normal and chordwise force coefficients obtained in reference 3, and presented as equations (48) and (49) in the previous section, may be utilized with a slight modification. Since equations (48) and (49) were written[3], before integration, in the form

$$C_N = \frac{C_1}{R_B} \int_0^{\ell} x \, dx$$

and

$$C_C = \frac{C_2}{R_B} \int_0^{\ell} x \, dx \ ,$$

where:

ℓ is the body length

and C_1 and C_2 are functions of δ, ω_u, and α,

the normal and chordwise force coefficients for the cone frustum may be defined by changing the limits of integration on these equations. Thus the equations for the minimum-drag cone frustum become:

$$C_N = \frac{C_1}{R_B} \int_{\ell_1}^{\ell} x \, dx$$

and

$$C_C = \frac{C_2}{R_B} \int_{\ell_1}^{\ell} x \, dx \qquad (55)$$

where: ℓ - the length of a cone having the same semivertex angle as the cone frustum (see Figure 5a).

and ℓ_1 - the length of that portion of the cone which is removed to form the cone frustum (see Figure 5a).

The two conditions, $\alpha \leq \delta$ and $\alpha > \delta$, must also be considered in defining the cone frustum force coefficients. Now, by comparing equations (54) and (55) it may be seen, from equations (48) and (49), that for the cone frustum

Case 1: $\alpha \leq \delta$

$$C_N = \sin \delta \cos \delta \sin 2\alpha \, \frac{\ell^2 - \ell_1^2}{R_B \ell} \qquad (56)$$

and

$$C_C = \tan \delta \left[2 \sin^2 \delta + \sin^2 \alpha \left(1 - 3 \sin^2 \delta\right) \right] \frac{\ell^2 - \ell_1^2}{R_B \ell}$$

Case 2: $\alpha > \delta$

$$C_N = \cos^2 \delta \sin 2\alpha \left\{ \frac{\omega_u + \frac{\pi}{2}}{\pi} + \frac{1}{3\pi} \cos \omega_u \left(\tan \delta \cot \alpha + 2 \cot \delta \tan \alpha\right) \right\} \frac{(\ell^2 - \ell_1^2)}{R_B \ell} \tag{57}$$

and

$$C_C = \left\{ \frac{\omega_u + \frac{\pi}{2}}{\pi} \left[2 \sin^2 \delta + \sin^2 \alpha \left(1 - 3 \sin^2 \delta\right) \right] + \frac{3}{4\pi} \cos \omega_u \sin 2\delta \sin 2\alpha \right\} \frac{(\ell^2 - \ell_1^2)}{R_B \ell} \tag{57}$$

Now substituting equations (56) and (57) into equations (50), the following equations for the cone frustum lift and drag coefficients are obtained:

Case 1: $\alpha \leq \delta$

$$C_L = \frac{(\ell^2 - \ell_1^2)}{R_B \ell} \tan \delta \left\{ \sin \alpha \left(2 - 3 \sin^2 \alpha\right) + \sin^2 \delta \left(5 \sin^3 \alpha - 4 \sin \alpha\right) \right\}$$

and

$$C_D = \frac{(\ell^2 - \ell_1^2)}{R_B \ell} \tan \delta \left\{ 3 \sin^2 \alpha \cos \alpha + \sin^2 \delta \cos \alpha \left(2 - 5 \sin^2 \alpha\right) \right\} \tag{58}$$

Case 2: $\alpha > \delta$

$$C_L = \frac{(\ell^2 - \ell_1^2)}{R_B \ell} \left\{ \frac{(\omega_u + \frac{\pi}{2})}{\pi} \left[2 \sin \alpha \left(1 - 2 \sin^2 \delta\right) + \sin^3 \alpha \left(5 \sin^2 \delta - 3\right) \right] + \frac{\cos \omega_u}{\pi} \left[\frac{2}{3} \cos^2 \delta \sin \alpha \cos^2 \alpha \left(\tan \delta \cot \alpha + 2 \cot \delta \tan \alpha\right) - \frac{3}{2} \sin 2\delta \sin^2 \alpha \cos \alpha \right] \right\}$$

$$C_D = \frac{(\ell^2 - \ell_1^2)}{R_B \ell}\left\{ \frac{(\omega_u + \frac{\pi}{2})}{\pi}\left[\sin^2 \alpha \cos \alpha \,(3 - \sin^2 \delta)\right] + \frac{\cos \omega_u}{\pi}\left[\frac{3}{2} \sin 2\delta \sin \alpha \cos^2 \alpha + \frac{2}{3} \cos^2 \delta \sin^2 \alpha \cos \alpha \,(\tan \delta \cot \alpha + 2 \cot \delta \tan \alpha)\right]\right\}. \quad (59)$$

Note that the above expressions, for the lift and drag coefficients, do not include the contribution of the flat nose of the cone frustum. The aerodynamic characteristics of a flat disk are relatively simple in form and will merely be stated here. Thus, for the case of a flat circular disk, initially normal to the flow direction, the lift and drag coefficients are:

$$C_L = -2 \sin \alpha \cos^2 \alpha$$

and $$C_D = 2 \cos^3 \alpha \quad . \quad (60)$$

The above coefficients are, however, based on the area of the flat disk itself. To obtain the contribution of this flat plate to the total lift and drag coefficients for the cone frustum, it is necessary to write equations (60) in terms of the cone frustum base area, or:

$$C_L = -2 \left(\frac{R_o}{R_B}\right)^2 \sin \alpha \cos \alpha$$

and $$C_D = 2 \left(\frac{R_o}{R_B}\right)^2 \cos^3 \alpha \quad (61)$$

where R_o is the radius of the nose piece (see Figure 5a).

The total Newtonian lift and drag coefficients for the cone frustum are obtained by simply adding the effect of the flat plate nose to that of the frustum shell. That is, the total aerodynamic force coefficients for the cone frustum are:

Case 1: $\alpha \leq \delta$

$$C_L = \frac{(\ell^2 - \ell_1^2)}{R_B \ell} \tan\delta \left\{ \sin\alpha\,(2 - 3\sin^2\alpha) + \sin^2\delta\,(5\sin^3\alpha - 4\sin\alpha) \right\} - 2\left(\frac{R_o}{R_B}\right)^2 \sin\alpha\cos^2\alpha$$

and

$$C_D = \frac{(\ell^2 - \ell_1^2)}{R_B \ell} \tan\delta \left\{ 3\sin^2\alpha\cos\alpha + \sin^2\delta\cos\alpha\,(2 - 5\sin^2\alpha) \right\} + 2\left(\frac{R_o}{R_B}\right)^2 \cos^3\alpha \qquad (62)$$

Case 2: $\alpha > \delta$

$$C_L = \frac{(\ell^2 - \ell_1^2)}{R_B \ell} \left\{ \frac{\omega_u + \frac{\pi}{2}}{\pi} \left[2\sin\alpha\,(1 - 2\sin^2\delta) + \sin^3\alpha\,(5\sin^2\delta - 3) \right] + \frac{\cos\omega_u}{\pi} \left[\frac{2}{3}\cos^2\delta\sin\alpha\cos^2\alpha\,(\tan\delta\cot\alpha + 2\cot\delta\tan\alpha) - \frac{3}{2}\sin 2\delta\sin^2\alpha\cos\alpha \right] \right\} - 2\left(\frac{R_o}{R_B}\right)^2 \sin\alpha\cos^2\alpha$$

and

$$C_D = \frac{(\ell^2 - \ell_1^2)}{R_B \ell} \left\{ \frac{\omega_u + \frac{\pi}{2}}{\pi} \left[\sin^2\alpha\cos\alpha\,(3 - \sin^2\delta) \right] + \frac{\cos\omega_u}{\pi} \left[\frac{3}{2}\sin 2\delta\sin\alpha\cos^2\alpha + \frac{2}{3}\cos^2\delta\sin^2\alpha\cos\alpha\,(\tan\delta\cot\alpha + 2\cot\delta\tan\alpha) \right] \right\} + 2\left(\frac{R_o}{R_B}\right)^2 \cos^3\alpha \,. \qquad (63)$$

The above equations are solved for the specific case of the minimum-drag cone frustum ($\delta = 31.7^\circ$ and $R_o = 0.3824\ R_B$) and plotted as a function of angle of attack in Figures 8 and 9.

Having now obtained the aerodynamic force coefficients for the bodies under investigation, the next development will entail a study of the stability derivatives for each. The stability derivatives, defined in the next section, are associated with stability about the transverse, or pitch, axis of a body.

Stability Parameters for Small Angle of Attack

At small angles of attack it may be assumed that the angle ω_u is a constant of magnitude $\frac{\pi}{2}$. Applying this assumption Toback and Wehrend[2] have developed general expressions for the stability derivatives associated with pitch stability. These are:

$$C_{N_\alpha} = \frac{2\pi}{S} \int_0^{\ell} R(x) \sin 2\psi \, dx \tag{64a}$$

$$C_{N_q} = \frac{2\pi}{S} \int_0^{\ell} R(x) \left[\frac{x}{\ell} \sin 2\psi + \frac{2\,R(x)}{\ell} \sin^2\psi \right] dx - \frac{x_o}{\ell} C_{N_\alpha} \tag{64b}$$

$$C_{M_\alpha} = \frac{-2\pi}{S\ell} \int_0^{\ell} \left[x\,R(x) + \tan\psi\, R^2(x) \right] \sin 2\psi \, dx + \frac{x_o}{\ell} C_{N_\alpha} \tag{64c}$$

$$C_{M_q} = \frac{-2\pi}{S\ell} \int_0^{\ell} \left[x\,R(x) + \tan\psi\, R^2(x) \right] \left[\frac{x}{\ell} \sin 2\psi + 2\frac{R(x)}{\ell} \sin^2\psi \right] dx + \frac{x_o}{\ell} C_{N_{q_o}} - \frac{x_o}{\ell} C_{M_{\alpha_o}} - \left(\frac{x_o}{\ell}\right)^2 C_{N_\alpha} \tag{64d}$$

where: S = body base area, πR_B^2

$R(x)$ = radius of the body in the y-z plane (see Figure 4).

ψ = slope of the body meridian curve, and is positive in sign (see Figure 4).

ℓ = body length

x_o = body center of gravity location measured from the origin of the coordinate system. (see Figure 4).

$C_{N_{q_o}}$, $C_{M_{\alpha_o}}$ = values of C_{N_q} and C_{M_α} for which x_o is taken to be zero.

The stability derivatives for each of the bodies under investigation will now be defined from equations (64).

Hemisphere

Equations (64) may be rewritten, for the special case of the hemisphere, by employing a change of variable. Utilizing the following relations which exist between the terms in these equations and the hemispherical coordinate system:

$$\begin{aligned} R(x) &= R_B \sin\theta \ , \\ x &= R_B - R_B \cos\theta \ , \\ \psi &= \frac{\pi}{2} - \theta \ , \end{aligned} \qquad (65)$$

and $\ell = R_B$;

Noting that the range of integration, for θ, must be changed to zero to $\frac{\pi}{2}$; then equations (64) become:

$$C_{N_\alpha} = 4 \int_0^{\frac{\pi}{2}} \sin^3 \theta \cos \theta \, d\theta \quad , \tag{66a}$$

$$C_{N_q} = 4 \int_0^{\frac{\pi}{2}} \sin^3 \theta \cos \theta \, d\theta - \frac{x_o}{R_B} \, , \tag{66b}$$

$$C_{M_\alpha} = - 4 \int_0^{\frac{\pi}{2}} \sin^3 \theta \cos \theta \, d\theta + \frac{x_o}{R_B} \, , \tag{66c}$$

and

$$C_{M_q} = - 4 \int_0^{\frac{\pi}{2}} \sin^3 \theta \cos \theta \, d\theta + \frac{x_o}{R_B} C_{N_{q_o}} - \frac{x_o}{R_B} C_{M_{\alpha_o}} - \left(\frac{x_o}{R_B}\right)^2 C_{N_\alpha} \, . \tag{66d}$$

Upon carrying out the indicated integration, the above stability derivatives are obtained as functions of $\frac{x_o}{R_B}$ only. That is,

$$\begin{aligned} C_{N_\alpha} &= 1.0 \, , \\ C_{N_q} &= 1 - \frac{x_o}{R_B} \, , \\ C_{M_\alpha} &= \frac{x_o}{R_B} - 1 \, , \end{aligned} \tag{67}$$

and

$$C_{M_q} = \frac{2 x_o}{R_B} - 1 - \left(\frac{x_o}{R_B}\right)^2 \, .$$

Cone

For the special case of a cone, equations (64) may be simplified by substituting the following quantities:

$$\psi = \delta = 45 \text{ degrees} ,$$
$$R(x) = x \tan \delta = x , \tag{68}$$
$$\ell = R_B .$$

With these substitutions the stability derivatives simplify to,

$$C_{N_\alpha} = \frac{2}{R_B^2} \int_0^{R_B} x \, dx , \tag{69a}$$

$$C_{N_q} = \frac{4}{R_B^3} \int_0^{R_B} x^2 \, dx - \frac{x_o}{R_B} C_{N_\alpha} , \tag{69b}$$

$$C_{M_\alpha} = \frac{-4}{R_B^3} \int_0^{R_B} x^2 \, dx + \frac{x_o}{R_B} C_{N_\alpha} , \tag{69c}$$

and

$$C_{M_q} = \frac{-4}{R_B^4} \int_0^{R_B} x^3 \, dx + \frac{x_o}{R_B} C_{N_{q_o}} - \frac{x_o}{R_B} C_{M_{\alpha_o}} - \left(\frac{x_o}{R_B}\right)^2 C_{N_\alpha} . \tag{69d}$$

Integration of the above equations yields the following results for the stability derivatives, in terms of $\frac{x_o}{R_B}$:

$$C_{N_\alpha} = 1.0 , \tag{70a}$$

$$C_{N_q} = \frac{4}{3} - \frac{x_o}{R_B} , \tag{70b}$$

$$C_{M_\alpha} = \frac{x_o}{R_B} - \frac{4}{3} \quad , \tag{70c}$$

and

$$C_{M_q} = -2 + \frac{8}{3}\,\frac{x_o}{R_B} - \left(\frac{x_o}{R_B}\right)^2 \quad . \tag{70d}$$

Cone Frustum

The stability derivatives for the cone frustum may be obtained in much the same manner as for the cone. Treating the cone frustum as a cone, but changing the lower limit of integration to properly describe the frustum, equations (64) are simplified by substituting the following quantities:

$$\begin{aligned} \psi &= \delta = 31.7 \text{ degrees}, \\ \ell &= R_B/\tan\delta, \\ \ell_1 &= R_o/\tan\delta, \\ R_o &= 0.3824\, R_B \ . \end{aligned} \tag{71}$$

Thus, equations (64) may be written in the following forms,

$$C_{N_\alpha} = \frac{4\sin^2\delta}{R_B^2} \int_{\ell_1}^{\ell} x\,dx \ , \tag{72a}$$

$$C_{N_q} = \frac{4\tan^2\delta}{R_B^2} \int_{\ell_1}^{\ell} x^2\,dx - \frac{x_o}{\ell}\, C_{N_\alpha} \ , \tag{72b}$$

$$C_{M_\alpha} = \frac{-4}{R_B^2}\tan^2\delta \int_{\ell_1}^{\ell} x^2\,dx + \frac{x_o}{\ell}\, C_{N_\alpha} \ , \tag{72c}$$

and

$$C_{M_q} = \frac{-4\tan^2\delta}{R_B^2 \quad ^2\cos^2\delta}\int_{\ell_1}^{\ell} x^3\,dx + \frac{x_o}{\ell}C_{N_{q_o}} - \frac{x_o}{\ell}C_{M_{\alpha_o}} - \left(\frac{x_o}{\ell}\right)^2 C_{N_\alpha} . \qquad (72d)$$

Upon carrying out the indicated integrations, and after substituting the limits, equations (72) reduce to,

$$C_{N_\alpha} = 1.2361 , \qquad (73a)$$

$$C_{N_q} = 1.2588 - 0.7634\frac{x_o}{R_B} , \qquad (73b)$$

$$C_{M_\alpha} = -1.2588 + 0.7634\frac{x_o}{R_B} , \qquad (73c)$$

and

$$C_{M_q} = -1.3146 + 1.6878\frac{x_o}{R_B} - 0.4715\left(\frac{x_o}{R_B}\right)^2 . \qquad (73d)$$

The stability derivatives have now been determined for small angles of attack. Numerical values of these quantities are presented in Table 3 for each of three physical body conditions described in the following section. These values will be applied later in determining the static and dynamic stability of the body types under investigation.

For large angles of attack the pitching velocity must be considered. Also, the angle, ω_u, can no longer be assumed a constant, as is demonstrated in the following section.

Stability Parameters for an Angle of Attack of 45 Degrees

General expressions for the stability derivatives have been obtained for the high angle of attack condition[2]. In this thesis the specific angle of attack of 45 degrees has been chosen since a closed form solution for C_{N_q} and C_{M_q} is not obtainable for the hemisphere at angles of attack other than zero degrees, 45 degrees, and 90 degrees. An angle of attack of 90 degrees will not be studied, however, due to the appearance of singularities in the stability parameters which lead to asymptotic solutions not sufficiently general for application to the present investigation.

The stability derivatives as given in reference 2, for high angles of attack are:

$$C_{N_\alpha} = -\frac{2}{S}\int_0^{x_u} R(x)\, H\,(x, \alpha, q)\, dx\,, \tag{74a}$$

$$C_{N_q} = -\frac{2}{S}\int_0^{x_u} R(x)\, J\,(x, \alpha, q)\, dx\,, \tag{74b}$$

$$C_{M_\alpha} = \frac{2}{S}\int_0^{x_u}\left[(x - x_o)\, R(x) + \tan\psi\, R^2(x)\right] H(x, \alpha, q)\, dx, \tag{74c}$$

and

$$C_{M_q} = \frac{2}{S}\int_0^{x_u}\left[(x - x_o)\, R(x) + \tan\psi\, R^2(x)\right] J(x, \alpha, q)\, dx, \tag{74d}$$

where:

$$H(x, \alpha, q) = \left[\frac{\omega_u}{2} - \frac{\sin 2\,\omega_u}{4} + \frac{\pi}{4}\right]\frac{\partial B}{\partial \Delta\,\alpha} - \frac{2}{3}\cos\,\omega_u\,(\sin^2\,\omega_u + 2)\,\frac{\partial G}{\partial\,\Delta\,\alpha}\,,$$

$$J(x, \alpha, q) = \left[\frac{\omega_u}{2} - \frac{\sin 2\omega_u}{4} + \frac{\pi}{4}\right] \frac{\partial B}{\partial \frac{\Delta q \ell}{V}} - \frac{2}{3} \cos \omega_u (\sin^2 \omega_u + 2) \frac{\partial G}{\partial \frac{\Delta q \ell}{V}},$$

and where: $$\frac{\partial B}{\partial \Delta \alpha} = -2 \sin 2\psi \sec^2 \alpha ,$$

$$\frac{\partial G}{\partial \Delta \alpha} = \frac{q \ell}{V} \sec^2 \alpha \left[\frac{R_B}{\ell} \sin 2\psi + 2 \frac{(x - x_o)}{\ell} \cos^2 \psi\right] + 2 \tan \alpha \sec^2 \alpha \cos^2 \psi ,$$

$$\frac{\partial B}{\partial \frac{\Delta q \ell}{V}} = -2 \left[2 \frac{R_B}{\ell} \sin^2 \psi + \frac{(x - x_o)}{\ell} \sin 2\psi\right] ,$$

and

$$\frac{\partial G}{\partial \frac{\Delta q \ell}{V}} = 2 \frac{q}{V} \left[\frac{R_B}{\ell} \sin \psi + \frac{(x - x_o)}{\ell} \cos \psi\right]^2 + \tan \alpha \left[\frac{R_B}{\ell} \sin 2\psi + 2 \frac{(x - x_o)}{\ell} \cos^2 \psi\right] .$$

In the above expressions the following parameters are:

ω_u = the angle in the y-z plane at which the pressure coefficient goes to zero for a given value of x.

x_u = the maximum value of x on that portion of the body which "sees" the flow.

q = pitching velocity.

V = velocity in the axial direction of the body

$\bar{q} = \frac{q \ell}{V}$ = dimensionless pitching velocity.

The above equations will be solved, for each body under investigation here, in the following sections.

Hemisphere

For the case of the hemisphere the same transformations will be applied to the general equations (74) as were applied in the previous section. However, the term ω_u is no longer a constant since the entire surface of the hemisphere is not covered by the flow. For an angle of attack of 45 degrees, ω_u has a constant value of $\frac{\pi}{2}$ for a range of θ from zero degrees to 45 degrees. For values of θ between 45 degrees and 90 degrees ω_u assumes the value $\sin^{-1}(\cot \theta)$. Therefore the integration of the stability derivatives must be separated into two integrals with limits on θ of zero to $\frac{\pi}{4}$ and $\frac{\pi}{4}$ to $\frac{\pi}{2}$ respectively. Applying the previously discussed transformations to equations (74), and separating into two integrals, the following equations are obtained:

$$C_{N_\alpha} = 8 \int_0^{\frac{\pi}{4}} \sin^3 \theta \cos \theta \, d\theta + \frac{8}{\pi} \int_{\frac{\pi}{4}}^{\frac{\pi}{2}} \left\{ \left[\sin^{-1}(\cot \theta) - \cot \theta \sqrt{1 - \cot^2 \theta} + \frac{\pi}{2} \right] \sin^3 \theta \cos \theta + \frac{2}{3} \sqrt{1 - \cot^2 \theta} \, (2 + \cot^2 \theta) \sin^2 \theta \left[\sin^2 \theta + \bar{q} \cos \theta (1 - \sin \theta) + \bar{q} \sin \theta \left(1 - \frac{x_o}{R}\right) \right] \right\} d\theta \tag{75a}$$

$$C_{N_q} = 4 \int_0^{\frac{\pi}{4}} \left\{ \sin^2\theta \cos^2\theta \,(1 - \sin\theta) + \sin^3\theta \cos\theta \,(1 - \frac{x_o}{R_B}) \right\} d\theta$$

$$+ \frac{4}{\pi} \int_{\frac{\pi}{4}}^{\frac{\pi}{2}} \left\{ \left[\sin^{-1}(\cot\theta) - \cot\theta \sqrt{1 - \cot^2} + \frac{\pi}{2} \right] \left[\sin^2\theta \cos^2\theta \,(1 - \right.\right.$$

$$\left.\left. \sin\theta) + \sin^3\theta \cos\theta \,(1 - \frac{x_o}{R_B}) \right] + \frac{2}{3} \sin^2\theta \sqrt{1 - \cot^2\theta} \,(2 + \right.$$

$$\left. \cot^2\theta) \left[\sin\theta \cos\theta \,(1 - \sin\theta) + \sin^2\theta \,(1 - \frac{x_o}{R_B}) + \bar{q} \left(\cos\theta \left[1 - \right.\right.\right.$$

$$\left.\left.\left. \sin\theta \right] + \sin\theta \left[1 - \frac{x_o}{R_B} \right] \right)^2 \right] \right\} d\theta \qquad (75b)$$

$$C_{M_\alpha} = \frac{x_o - R_B}{R_B} \, C_{N_\alpha} \,, \qquad (75c)$$

and

$$C_{M_q} = \frac{x_o - R_B}{R_B} \, C_{N_q} \,. \qquad (75d)$$

Carrying out the indicated integrations, the above equations reduce, upon substitution of the limits, to

$$C_{N_\alpha} = 2.3918 + (\bar{q})\, 0.9131 - 0.8488 \, \frac{x_o}{R_B} \,, \qquad (76a)$$

$$C_{N_q} = 0.6983 + 0.5224 \, \bar{q} - (0.8236 + 0.4829 \, \bar{q}) \, \frac{x_o}{R_B} \qquad (76b)$$

$$C_{M_\alpha} = -0.9131 \, \bar{q} - 2.3918 + \frac{x_o}{R_B} \,(2.3918 + 1.761 \, \bar{q} - 0.8488 \, \frac{x_o}{R_B} \, \bar{q}), \qquad (76c)$$

and

$$C_{M_q} = -0.5224\,\bar{q} - 0.6983 + \frac{x_o}{R_B}(1.5219 + 1.0053\bar{q}) - \left(\frac{x_o}{R_B}\right)^2 (0.8236 + 0.4829\,\bar{q}) \quad . \tag{76d}$$

Cone

In the case of the cone the term ω_u is a constant and is found to be $\sin^{-1}(\tan \delta)$. Since the cone under investigation here has a semi-angle of 45 degrees, the entire surface is covered by the flow and ω_u has a value of $\frac{\pi}{2}$. Thus equations (74) reduce to a relatively simple form when the previously discussed transformations are applied. That is,

$$C_{N_\alpha} = \frac{4}{R_B^2} \int_0^{R_B} x\,dx \,, \tag{77a}$$

$$C_{N_q} = \frac{2}{R_B^2} \int_0^{R_B} \left(x + \frac{x^2}{R_B} - \frac{x_o\,x}{R_B}\right) dx \,, \tag{77b}$$

$$C_{M_\alpha} = \frac{-4}{R_B^3} \int_0^{R_B} (2x^2 - x_o\,x)\,dx \,, \tag{77c}$$

and

$$C_{M_q} = \frac{-2}{R_B^3} \int_0^{R_B} \left[2x^2\left(1 + \frac{x}{R_B}\right) - x_o\,x\left(1 + \frac{3x}{R_B} - \frac{x_o}{R_B}\right)\right] dx \,. \tag{77d}$$

After integrating and substituting the limits, the above equations reduce to

$$C_{N_\alpha} = 2.0 \,, \tag{78a}$$

$$C_{N_q} = \frac{5}{3} - \frac{x_o}{R_B} \quad , \tag{78b}$$

$$C_{M_\alpha} = \frac{-8}{3} + 2\frac{x_o}{R_B} \quad , \tag{78c}$$

and

$$C_{M_q} = \frac{-5}{3} + 3\left(\frac{x_o}{R_B}\right) - \left(\frac{x_o}{R_B}\right)^2 \quad . \tag{78d}$$

Cone Frustum

Again the cone frustum may be treated in a manner similar to the cone. Upon substitution of the appropriate transformations for the cone frustum, equations (74) reduce to:

$$C_{N_\alpha} = \frac{16}{\pi R_B^2} \int_{\ell_1}^{\ell} x \tan\delta \left\{ \left[\cos\delta \left(\frac{\omega_u}{2} + \frac{\sin 2\,\omega_u}{4} + \frac{\pi}{4} \right) \sin\delta + \frac{2 + \tan^2\delta}{3} \cos\,\omega_u \cos\delta \right] + \frac{\bar{q}}{3} \cos\,\omega_u \left[\frac{R_B}{\ell} \sin\delta + \frac{(x - x_o)}{\ell} \cos\delta \right] \cos\delta \right\} dx \quad , \tag{79a}$$

$$C_{N_q} = \frac{8}{\pi R_B^2} \int_{\ell_1}^{\ell} x \tan\delta \left\{ \sin\delta \cos\delta \left[\left(\frac{\omega_u}{2} + \frac{\sin 2\,\omega_u}{4} + \frac{\pi}{4} \right) \frac{(x - x_o)}{\ell} + \frac{(2 + \tan^2\delta)}{3} \frac{R_B}{\ell} \cos\,\omega_u \right] + \left(\frac{\omega_u}{2} + \frac{\sin 2\,\omega_u}{4} + \frac{\pi}{4} \right) \frac{R_B}{\ell} \sin^2\delta + \frac{1}{3}(2 + \tan^2\delta) \frac{(x - x_o)}{\ell} \cos^2\delta \cos\,\omega_u + \frac{\bar{q}}{3} \cos\,\omega_u (2 + \tan^2\delta) \left[\frac{R_B}{\ell} \tan\delta + \frac{(x - x_o)}{\ell} \cos\,\omega_u \right]^2 \right\} dx \quad , \tag{79b}$$

$$C_{M_\alpha} = \frac{-8}{\pi R_B^2 \ell} \int_{\ell_1}^{\ell} \left[(x - x_o)x \tan\delta + x^2 \tan^3\delta\right]\left\{\left(\frac{\omega_u}{2} - \frac{\sin 2\omega_u}{4} + \frac{\pi}{4}\right)\sin 2\delta + \frac{1}{3}\left[\cos\omega_u (2 + \tan^2\delta)\right]\left[\frac{-}{q}\left(\frac{R_B}{\ell}\sin 2\delta + \frac{2(x - x_o)}{\ell}\cos^2\delta\right) + 2\cos^2\delta\right]\right\} dx \quad (79c)$$

and

$$C_{M_q} = \frac{-4}{\pi R_B^2 \ell} \int_{\ell_1}^{\ell} x \tan\delta(x - x_o + x\tan^2\delta)\left\{\left(\omega_u - \frac{\sin 2\omega_u}{2} + \frac{\pi}{2}\right)\left(\frac{R_B}{\ell}\sin^2\delta + \frac{(x - x_o)}{\ell}\sin\delta\cos\delta\right) - \frac{1}{3}\cos\omega_u (2 + \sin^2\omega_u)\left[2\,\bar{q}\,\left(\frac{R_B}{\ell}\sin\delta + \frac{(x - x_o)}{\ell}\cos\delta\right)^2 + \frac{R_B}{\ell}\sin 2\delta + \frac{2(x - x_o)}{\ell}\cos^2\delta\right]\right\} dx \quad (79d)$$

where: $\omega_u = \sin^{-1}(\tan\delta)$

Note that a value of ω_u has not been substituted into the above equations since this parameter will be varied later to ascertain the effect of the ratio of the radii of the front and rear faces of the cone frustum on the stability. For the case of the previously discussed minimum-drag cone frustum, equations (79) become, upon integrating and substituting of limits,

$$C_{N_\alpha} = 2.9686 + \bar{q}\;\; 2.1562 - 0.9835\;\; \frac{x_o}{R_B} \quad , \quad (80a)$$

$$C_{N_q} = 1.66 + 1.267\,\bar{q} - \frac{x_o}{R_B}(0.917 - 0.6891\,\bar{q}), \qquad (80b)$$

$$C_{M_\alpha} = \frac{x_o}{R_B}\left[1.833 + 2.3336\,\bar{q} - 0.6073\,\bar{q}\,\frac{x_o}{R_B}\right] - 0.835 - 1.147\,\bar{q}, \qquad (80c)$$

and

$$C_{M_q} = \frac{x_o}{R_B}\left[0.4429 + 1.3713\,\bar{q}\right] - \left(\frac{x_o}{R_B}\right)^2 (0.2831 + 0.3569\,\bar{q}) - 0.882\,\bar{q} - 1.787 \quad . \qquad (80d)$$

Equations (80) complete the investigation of the stability derivatives. Note that these equations are written in terms of $\frac{x_o}{R_B}$ only. Numerical values of the stability derivatives, for each of three physical conditions described in the next section are listed in Table 3.

Center of Gravity Location and Radius of Gyration.

Before the static and dynamic stability is studied it will be necessary to determine both the location of the center of gravity and radius of gyration for the three bodies under consideration. For each body type three physical conditions, or mass distributions, will be assumed; these are:

1. A solid, homogeneous body.
2. A body shell with an open base.
3. A body shell with a flat disk closing the base.

The general procedure followed is to apply the integral calculus to elemental mass segments to obtain the center of

gravity location and radius of gyration for each body. For convenience, the method employed will be defined for the general case and the actual values tabulated. (See Table 2).

The location of the center of gravity is determined in the following manner. The definition of the center of gravity is,

$$x_o M = \int_0^L x \, dM \tag{81}$$

where:

x_o = the distance from the coordinate origin to the center of gravity (see Figure 5b).

M = the total mass of the body.

In the above equation the elemental mass may be written as:

$$dM = \rho \pi r^2 dx \tag{82}$$

where:

r = the radius of the body of revolution for a given value of x. (See Figure 5b).

ρ = the mass density of the body (here assumed constant).

For the bodies considered it is a relatively simple matter to relate the variables r and x. The integration, indicated in equation (81), has been performed and the values of $\frac{x_o}{R_B}$ are listed in Table 2.

In order to obtain the radius of gyration for these bodies it is necessary to define the mass moment of inertia, which is related to the radius of gyration of a body, by the expression

$$k = \sqrt{\frac{I}{M}} \quad . \tag{83}$$

The mass moment of inertia, I, may be expressed about a general transverse axis as

$$I = \int \bar{r}^2 \, dM \quad . \tag{84}$$

From consideration of the elemental mass segment depicted in Figure 5b, it is seen that a triple integration process must be followed in defining the mass moment of inertia. Thus, the radius of gyration for a general body of revolution about the transverse axis through the body center of gravity (the pitch axis) can be written as:

$$k^2 = \frac{2\rho \int_0^L \int_0^{R(x)} \int_{-\frac{\pi}{2}}^{\frac{\pi}{2}} \left[(L - x)^2 + (r \sin B)^2 \right] r \, dB \, dr \, dx - \bar{x}^2}{M} \tag{85}$$

where: M is the total body mass.

The above equation has been solved for each of the bodies under investigation and values of radius of gyration are listed in Table 2.

Having derived expressions for the stability derivatives and determined the center of gravity location and radii of gyration for the three bodies under investigation, the static and dynamic stability can be studied. In the next section the static stability is considered.

Static Stability

For static stability to exist, a disturbance, from equilibrium, must create forces or moments within the system that tend to restore the system to the equilibrium position. The stability derivatives defined in the previous section are associated with motion about the transverse, or pitch, axis through the center of gravity of the body. Since the stability of motion about this axis is of primary importance in the study of reentry problems, it is quite logical that it be included in this thesis.

Allen[5] has developed expressions by which the static and dynamic stability can be defined. This was done by considering the time differential equation of motion, about the pitch axis, of an axially symmetric body of revolution entering the earth's atmosphere. For the case of static stability, it was found[5] that if the following inequality exists,

$$- C_{M_\alpha} + C_{L_\alpha} \beta \sin \theta_E > 0 \qquad (86)$$

a body of revolution is stable for motions about its pitch axis. The second term in equation (86) is negligible since the quantity, β, defined in the expression relating the air density at an altitude y (in feet) to the air density at sea level:

$$\rho = \rho_o e^{-\beta y}$$

where: ρ_o = sea level air density,

must be much less than unity for altitudes of the order of magnitude of 1000 feet or greater. Therefore, it follows that an axially symmetric body of revolution is statically stable, about the pitch axis, if the stability derivative C_{M_α} is negative.

With the condition of stability defined, the three specific cases of interest to this thesis will next be studied separately.

Hemisphere

For small angles of attack the term C_{M_α}, as obtained in equation (67c), is

$$C_{M_\alpha} = -1 + \frac{x_o}{R_B} \quad . \tag{67c}$$

Since $\frac{x_o}{R_B}$ must be less than unity for all physical conditions of the hemisphere, the hemisphere is statically stable at small angles of attack.

At an angle of attack of 45 degrees it is necessary to set the non-dimensional pitching velocity, $\bar{q}$, equal to zero in order to determine the static stability. For this condition,

$$C_{M_\alpha} = 2.3918 \ \frac{x_o}{R_B} - 2.3918 \tag{87}$$

The location of the center of gravity for a solid homogeneous hemisphere, as obtained from Table 2, is at the point

$$\frac{x_o}{R_B} = \frac{5}{8}$$

For this value of $\frac{x_o}{R_B}$

$$C_{M_\alpha} = - 0.8969 \qquad (88)$$

and the solid, homogeneous hemisphere is therefore statically stable.

Similarly, for the hemispherical shell without a base plate

$$\frac{x_o}{R_B} = 0.5 \quad \text{and} \quad C_{M_\alpha} = - 1.1959 \ , \qquad (89)$$

a statically stable configuration.

For the hemispherical shell with a base plate

$$\frac{x_o}{R_B} = \frac{2}{3} \quad \text{and} \quad C_{M_\alpha} = - 0.7972 \qquad (90)$$

indicating a statically stable body type.

It is seen that for the case of the hemispherical shell with no base plate the body exhibits the highest degree of static stability both at small angles of attack and at an angle of attack of 45 degrees.

Cone

At small angles of attack the stability derivative, C_{M_α}, for the cone can be written, from equation (70c), as

$$C_{M_\alpha} = \frac{x_o}{R_B} - \frac{4}{3} \ . \qquad (70c)$$

Noting the values of $\frac{x_o}{R_B}$, for the cone, in Table 2, it is seen that the cone is statically stable for all cases. Also it is self-evident that the conical shell without a base plate exhibits the greatest degree of stability.

At an angle of attack of 45 degrees, the value of C_{M_α} is

$$C_{M_\alpha} = \frac{2\,x_o}{R_B} - \frac{8}{3}$$

as given in equation (78c).

Here again the cone is statically stable for all physical conditions investigated, and the conical shell, without a base plate, exhibits the greatest stability.

Minimum-Drag Cone Frustum

At small angles of attack the stability derivative, C_{M_α}, as obtained in equation (73c) is,

$$C_{M_\alpha} = -\,1.2588 + 0.7634\ \frac{x_o}{R_B}\ . \qquad (73c)$$

The cone frustum is seen to be statically stable since $\frac{x_o}{R_B}$ must be less than unity for all practical mass distributions. From the values of $\frac{x_o}{R_B}$ presented in Table 2, the cone frustum shell, without a base plate, exhibits the greater stability.

In addition it is seen that varying the ratio of the cone frustum radii results in a change in the stability index. Specifically, this body type becomes more stable (statically) as the radius of the forward face, R_o, approaches zero (i.e. as the frustum approaches a cone).

The term, C_{M_α}, for the cone frustum, at an angle of attack of 45 degrees, as obtained in equation (80c) is:

$$C_{M_\alpha} = 1.833 \frac{x_o}{R_B} - 0.835 \quad .$$

For the values of $\frac{x_o}{R_B}$ listed in Table 2 it is seen that the cone frustum is statically unstable for the three physical conditions investigated here. The least unstable configuration is the case of the cone frustum shell without a base plate.

Also it is seen that a change in the radius of the cone frustum nose leads to a change in stability. Explicitly, the cone frustum becomes more stable (statically) as the radius of the nose again approaches a value of zero.

The results of this investigation for static stability are summarized and presented in Table 4. In this table a positive sign indicates a stable configuration, and a negative sign indicates an unstable configuration.

Next, to carry the investigation of stability one step further the dynamic stability is studied.

Dynamic Stability

If, after disturbing a dynamical system from its equilibrium position, the subsequent motion eventually returns the system to the equilibrium position, the system is said to be dynamically stable. This general definition of dynamic stability indicates that it is most desirable to have dynamic stability of a system so that no external devices need be added to obtain stability.

Allen[5] presented a condition which must be satisfied for the dynamic stability of a system. This condition is stipulated by the inequality

$$C_D - C_{L_\alpha} + (C_{M_q} + C_{M_\alpha}) \left(\frac{R_B}{k}\right)^2 < 0 . \qquad (91)$$

In the above expression the term C_{M_α} is generally negligible for axially symmetric bodies of revolution. The condition which the three bodies under investigation must satisfy, for stability, is therefore

$$C_D - C_{L_\alpha} + C_{M_q} \left(\frac{R_B}{k}\right)^2 < 0 . \qquad (92)$$

Each of the bodies considered will now be tested to ascertain whether this condition is satisfied and/or under what restraints it will be satisfied.

Hemisphere

At small angles of attack the hemisphere exhibits the following previously defined characteristics:

$$C_D = 1.0$$
$$C_{L_\alpha} = 0 \qquad (93)$$
$$C_{M_q} = -\left(1 - \frac{x_o}{R_B}\right)^2$$

Substituting these values into equation (92) the stability condition becomes,

$$1 - \left(1 - \frac{x_o}{R_B}\right)^2 \left(\frac{R_B}{k}\right)^2 < 0 \quad . \tag{94}$$

Considering the values of $\frac{x_o}{R_B}$ and k^2, obtained from Table 2, it is seen that the hemisphere is dynamically unstable for the three mass distributions considered. Of these, the least unstable is the case of the hemispherical shell without a base plate.

At an angle of attack of 45 degrees the hemisphere was found to have the following characteristics,

$$C_D = 0.941$$

$$C_{L_\alpha} = -0.2652 \tag{95}$$

$$C_{M_q} = -0.6983 + 1.5219 \frac{x_o}{R_B} - 0.8236 \left(\frac{x_o}{R_B}\right)^2 \quad ;$$

which, upon substitution, reduce equation (92) to

$$0.6758 + \left[-0.6983 + 1.5219 \frac{x_o}{R_B} - 0.8236 \left(\frac{x_o}{R_B}\right)^2\right] \left(\frac{R_B}{k}\right)^2 < 0 \tag{96}$$

Applying the values of $\frac{x_o}{R_B}$ and k^2 from Table 2 it follows that the hemisphere is again dynamically unstable, with the least unstable configuration being that of the hemispherical shell without a base plate.

Cone

The pertinent parameters for the cone at small angle of attack are:

$$C_D = 1.0$$

$$C_{L_\alpha} = 0 \qquad (97)$$

$$C_{M_q} = -2 + \frac{8}{3}\left(\frac{x_o}{R_B}\right) - \left(\frac{x_o}{R_B}\right)^2$$

Therefore the governing stability condition becomes

$$1 + \left[-2 + \frac{8}{3}\left(\frac{x_o}{R_B}\right) - \left(\frac{x_o}{R_B}\right)^2\right]\left(\frac{R_B}{k}\right)^2 < 0 \,. \qquad (98)$$

It can be shown that the cone satisfies this relation for each physical condition considered. Also, the greatest degree of stability is obtained for the case of the solid, homogeneous cone.

Values of C_D, C_{L_α}, and C_{M_q} for the cone at an angle of attack of 45 degrees are:

$$C_D = 0.8839$$

$$C_{L_\alpha} = -0.5303 \qquad (99)$$

$$C_{M_q} = -\frac{5}{3} + 3\left(\frac{x_o}{R_B}\right) - \left(\frac{x_o}{R_B}\right)^2 \,.$$

Substitution of these values in equation (92) yields

$$1.4142 + \left[-\frac{5}{3} + 3\left(\frac{x_o}{R_B}\right) - \left(\frac{x_o}{R_B}\right)^2\right]\left(\frac{R_B}{k}\right)^2 < 0 \,. \qquad (100)$$

At an angle of attack of 45 degrees the cone is dynamically unstable to a lesser degree for the conical shell without a base

plate than for the other cases as may be demonstrated by substituting values of $\frac{x_o}{R_B}$ and k^2 from Table 2 into the above equation.

Cone Frustum

The minimum-drag cone frustum exhibits the following aerodynamic characteristics at small angles of attack:

$$\begin{aligned} C_D &= 0.763 \\ C_{L_\alpha} &= 0.585 \\ C_{M_q} &= -1.3146 + 1.6878 \frac{x_o}{R_B} - 0.4715 \left(\frac{x_o}{R_B} \right)^2 . \end{aligned} \tag{101}$$

Equation (92) becomes (upon substitution of these quantities):

$$0.178 + \left[-1.3146 + 1.6878 \left(\frac{x_o}{R_B} \right) - 0.4715 \left(\frac{x_o}{R_B} \right)^2 \right] \left(\frac{R_B}{k} \right)^2 < 0 \tag{102}$$

The above stability condition is satisfied for each of the physical conditions of the cone frustum as listed. This can be demonstrated by substituting the values of $\frac{x_o}{R_B}$ and k^2 obtained from Table 2 into equation (102).

The greatest degree of dynamic stability is obtained for the solid, homogeneous cone frustum. It can also be shown that as the radius of the nose of a cone frustum approaches that of its base (hence a cylinder) the degree of dynamic stability increases.

At an angle of attack of 45 degrees the pertinent parameters necessary to the determination of the dynamic stability of the cone frustum have been previously found to be:

$$C_D = 1.1884$$

$$C_{L_\alpha} = -\ 0.868 \qquad (103)$$

$$C_{M_q} = 0.4429\ \frac{x_o}{R_B} - 0.2831\ \left(\frac{x_o}{R_B}\right)^2 - 1.187\ .$$

Thus equation (92), with the above terms substituted for the variables, becomes

$$2.0564 + \left[-\ 1.787 + 0.4429\ \frac{x_o}{R_B} - 0.2831\ \left(\frac{x_o}{R_B}\right)^2\right]\ \left(\frac{R_B}{k}\right)^2 < 0\ . \qquad (104)$$

For this angle of attack condition it is seen that the cone frustum is dynamically stable. Again, the greatest degree of dynamic stability is produced by the solid, homogeneous cone frustum. Also, the degree of stability increases as the nose radius approaches the value of the base radius of the body (the limit case being the cylinder).

The static and dynamic stability of the bodies under investigation in this thesis have been defined. Also, both the static and dynamic stability of these configurations are presented in Table 4.

The results, obtained from this investigation, are discussed to some extent in the following section and various conclusions presented.

III. DISCUSSION OF RESULTS

Drag Coefficient

The Newtonian and Newtonian-plus-centrifugal drag coefficients, as obtained for the hemisphere, are presented for an angle of attack range from zero degrees to 90 degrees in Figure 6 and Table 1. In Figure 6 the upper curve is a plot of equation (13) and the lower curve is a plot of equation (42). It is of interest to point out that the maximum and minimum values of the hemisphere Newtonian drag coefficient are:

$$C_{D_{N_{max}}} = 1.0 \quad \text{at} \quad \alpha = 0 \text{ degrees}$$

$$C_{D_{N_{min}}} = 0.5 \quad \text{at} \quad \alpha = 90 \text{ degrees}$$

and the maximum and minimum values of the Newtonian-plus-centrifugal drag coefficient are:

$$C_{D_{N + C_{max}}} = 0.75 \quad \text{at} \quad \alpha = 0 \text{ degrees}$$

$$C_{D_{N + C_{min}}} = 0.375 \quad \text{at} \quad \alpha = 90 \text{ degrees}$$

Also, the Newtonian-plus-centrifugal coefficient is found to be constant for angles of attack less than or equal to 30 degrees

since the pressure coefficient acting on the "missing" area is zero for this range of angles of attack.

Consideration of centrifugal force effects is seen to decrease the hemisphere drag coefficient by a maximum of 25 percent at angles of attack of zero degrees and 90 degrees. The minimum relieving effect of the centrifugal forces is 23 percent at an angle of attack of 45 degrees. Therefore, the Newtonian-plus-centrifugal drag coefficient may be reasonably approximated by,

$$C_{D_{N+C}} = 0.75\ C_{D_N}$$

The two curves presented in Figure 6 are felt to be the upper and lower limits of the true drag coefficient for the hemisphere at any angle of attack. For low hypersonic speeds the true drag coefficient will approach the Newtonian value, while at high hypersonic speeds it will approach the Newtonian-plus-centrifugal value.

The Newtonian drag coefficients obtained for the inscribed cone and minimum-drag cone frustum are presented in Figure 9. It may be seen from this figure, and also from Figure 6, that the minimum-drag cone frustum exhibits a lesser drag coefficient than either the cone or the hemisphere, but only for angles of attack less than 35 degrees and for low hypersonic speeds. At high hypersonic speeds, where the drag coefficient for the hemisphere

approaches the Newtonian-plus-centrifugal value, the cone frustum exhibits a larger drag coefficient than the hemisphere throughout the entire angle of attack range.

Lift Coefficient

The hemisphere Newtonian and Newtonian-plus-centrifugal lift coefficients, equations (25) and (47), are presented in Figure 7 and Table 1. The Newtonian-plus-centrifugal lift coefficient has a value of zero for angles of attack less than or equal to 30 degrees since the centrifugal forces exactly counteract the effect of impact on the "missing" area. As the angle of attack increases above 30 degrees, the Newtonian impact forces overpower the centrifugal forces and a negative lift force is produced on the hemisphere.

It may also be seen from Figure 7 that the relieving effects of the centrifugal forces are much greater for the lift coefficient than for the drag coefficient. For instance, at an angle of attack of 90 degrees the centrifugal force effects decrease the lift coefficient by approximately 45 percent.

The two expressions obtained in this thesis for the hemisphere's lift coefficient are felt to be (at least) the upper and lower limits of the true lift coefficient at hypersonic speeds and angle of attack.

The Newtonian lift coefficient for the inscribed cone and minimum-drag cone frustum are presented in Figure 8. It is seen

that the minimum-drag cone frustum is the only configuration considered in this thesis which has a positive lift coefficient for any portion of the angle of attack range. Note however that for angles of attack greater than 55 degrees the lift coefficient for the cone frustum is more negative than that for the hemisphere.

From the preceeding discussion it may be seen that for a missile at fairly low hypersonic speeds and an angle of attack variation of less than plus or minus 35 degrees the minimum-drag cone frustum exhibits the more favorable aerodynamic characteristics. Thus, for these conditions, it would be desired to use this configuration for a missile nose shape. However, for a missile designed to fly at very high hypersonic speeds and a very large angle of attack variations (of the order of plus or minus 90 degrees) it would be desirable to use a hemispherical missile nose configuration.

Static Stability

The individual stability parameters are presented in Table 3. It is felt that it is unnecessary to discuss these quantities here except insofar as they affect the static and dynamic stability.

The static stability was shown to be a function of C_{M_α} only. Thus the values of C_{M_α} defined in Table 3 determines the static stability listed in Table 4 for the three body configurations investigated in this thesis. From Table 4 it may be seen that

all configurations are stable and that the minimum-drag cone frustum exhibits the greatest degree of static stability at small angles of attack. However, for an angle of attack of 45 degrees the inscribed cone frustum exhibits the greatest degree of static stability. In each case the thin shell without a base plate is the most stable body condition.

Dynamic Stability

The dynamic stability of each configuration is also presented in Table 4. For small angles of attack it is noted that the hemisphere is the only unstable configuration. At an angle of attack of 45 degrees the only stable configuration is the minimum-drag cone frustum. Also it is worthy of mention that the greatest degree of dynamic stability is exhibited by the solid, homogeneous body condition.

From this investigation of stability it appears that the cone frustum is the more desirable missile nose shape; even though the hemisphere was found to exhibit the more favorable aerodynamic characteristics over the entire range of angle of attack. Thus it would depend on which factors were the more critical for a missile design (stability or lift and drag) as to whether the hemisphere or the cone frustum would be the more desirable missile nose configuration. As has been shown here the cone is the median body both for stability and magnitude of

force coefficients. It is felt that considerations of aerodynamic heating and fabrication would lead to the selection of the hemisphere as the optimum missile nose configuration.

IV. CONCLUSIONS

The following conclusions may be drawn from this thesis:

1. The Newtonian lift and drag coefficients represent the upper limit of the actual force coefficients for the hemisphere, the inscribed cone, and the minimum-drag cone frustum at angles of attack.

2. The Newtonian-plus-centrifugal force coefficients represent the lower limit of the actual force coefficients for the hemisphere at angles of attack.

3. The Newtonian-plus-centrifugal drag coefficient, for the hemisphere, may be approximated by taking 75 percent of the Newtonian drag coefficient.

4. The angle of attack may be changed by as much as 30 degrees without appreciable change of the hemisphere's force coefficients.

5. The minimum-drag cone frustum exhibits the greatest degree of both static and dynamic stability.

6. The hemisphere exhibits the more favorable aerodynamic force coefficients.

7. The hemisphere is the more desirable missile nose configuration from the standpoint of a missile possessing a stabilizing afterbody and requiring a large angle of attack variation.

V. RECOMMENDATIONS

The results of the present thesis indicate that a study of the centrifugal force effects should be carried out for the cone frustum and the cone to determine their aerodynamic characteristics at high hypersonic Mach numbers. In addition, it is felt that experimental data would be of great aid in determining the accuracy of the force coefficient equations developed here.

VI. SUMMARY

In this thesis a study has been made of the aerodynamic characteristics of a hemisphere flying at high speeds. The lift and drag coefficients have been obtained for the hemisphere, at angles of attack, through the application of Newton's corpuscular theory. A correction has been applied to the coefficients to account for the effect of the centrifugal forces acting on the hemisphere due to flow curvature. The application of the above correction then yielded the Newtonian-plus-centrifugal lift and drag coefficients for the hemisphere. A study has also been made of the Newtonian force coefficients for the cone inscribed in the hemisphere, and the minimum-drag cone frustum having the same fineness ratio as the hemisphere. The results of this last study show that the cone frustum is the only body considered having a positive lift coefficient over any portion of the angle of attack range (zero to 40 degrees). In addition, the hemisphere's Newtonian drag coefficient is greater than that of the cone frustum only for angles of attack less than 35 degrees.

A study of the stability parameters C_{N_α}, C_{N_q}, C_{M_α}, and C_{M_q} has also been carried out in this thesis. Having defined these quantities for the hemisphere, cone, and the cone frustum, the static and dynamic stability of each body was investigated. From this investigation it was concluded that the minimum drag cone

frustum exhibits the greatest degree of (both) static and dynamic stability.

Three body conditions: a solid, homogeneous body; a shell body without a base plate; and a shell body with a base plate were considered in the stability study for each configuration. It was found that a shell body, without a base plate, exhibits the greater static stability for each case, but that a solid homogeneous body exhibits the greater dynamic stability for all stable configurations. However, the shell body without a base plate, was the more stable condition for the dynamically unstable configurations.

The results of this thesis indicate that the shell hemisphere would be the most favorable missile nose configuration of those considered. This is concluded since the hemisphere exhibits the more favorable force coefficients and the application of a missile afterbody would produce a stable missile configuration.

VII. ACKNOWLEDGEMENT

It is the desire of the author to express his sincere appreciation to and of the Aeronautical Engineering Department at the Virginia Polytechnic Institute for their patient assistance in the successful completion of this project.

VIII. BIBLIOGRAPHY

1. Ivey, H. R.; Klunker, B. E.; and Bowen, E. N.: A Method for Determining the Aerodynamic Characteristics of Two- and Three-Dimensional Shapes at Hypersonic Speeds. NACA TN No. 1613, July 1948.

2. Tobak, Murray; and Wehrend, William R.: Stability Derivatives of Cones at Supersonic Speeds. NACA TN No. 3788, September 1956.

3. Grimminger, G.; Williams, E. P.; and Young, G.B.W.: Lift on Inclined Bodies of Revolution in Hypersonic Flow. Journal of the Aeronautical Sciences, Vol. 17, No. 11, p. 675, November 1950.

4. Truitt, R. W.: Minimum-Drag Cone Frustum at Hypersonic Speeds. Journal of the Aero/Space Sciences, Vol. 25, No. 8, August 1958.

5. Allen, H. J.: Motion of a Ballistic Missile Angularly Misaligned with the Flight Path upon Entering the Atmosphere and its Effect upon Aerodynamic Heating, Aerodynamic Loads, and Miss Distance. NACA TN No. 4048, October 1957.

6. Charters, A. C.: Some Ballistic Contributions to Aerodynamics. Journal of the Aeronautical Sciences, Vol. 14, No. 3, p. 155, March 1947.

7. Charwat, A. R.: The Stability of Bodies of Revolution at Very High Mach Numbers. Jet Propulsion, p. 866, August 1957.

8. Eggers, Alfred J., Jr.; Allen, H. Julian; and Neice, Stanford E.: A Comparative Analysis of the Performance of Long Range Hypervelocity Vehicles. NACA TN No. 4046, 1957.

9. Friedrich, Hans R.; and Dore, Frank J.: The Dynamic Motion of a Missile Descending through the Atmosphere. Journal of the Aeronautical Sciences, Vol. 22, No. 9, September 1955.

The vita has been removed from the scanned document

TABLE 1

HEMISPHERE FORCE COEFFICIENTS

α	$C_{D_N} + C$	(-) $C_{L_N} + C$	C_{D_N}	(-) C_{L_N}
0	0.75000	0.0	1.0	- 0
1			1.0	- 0
2			1.0	- 0.00001
3			1.0	- 0.00004
4			1.0	- 0.00009
5			0.99999	- 0.00017
6			0.99998	- 0.00029
7			0.99997	- 0.00045
8			0.99993	- 0.00068
9			0.99988	- 0.00096
10			0.9998	- 0.0013
11			0.9998	- 0.0017
12			0.9997	- 0.0023
13			0.9995	- 0.0029
14			0.9993	- 0.0036
15			0.9991	- 0.0043
16			0.9989	- 0.0052
17			0.9986	- 0.0063
18			0.9982	- 0.0074
19			0.9978	- 0.0086
20			0.9972	- 0.0100
21			0.9966	- 0.0115
22			0.9960	- 0.0131
23			0.9953	- 0.0149
24			0.9946	- 0.0168
25			0.9936	- 0.0189
26			0.9925	- 0.0211
27			0.9913	- 0.0233
28			0.9901	- 0.0259
29			0.9886	- 0.0285
30	0.7500	- 0.0	0.9869	- 0.0313
31	0.7483	- 0.00007	0.9853	- 0.0342
32	0.7466	- 0.0003	0.9835	- 0.0372
33	0.7450	- 0.0005	0.9813	- 0.0404
34	0.7434	- 0.0009	0.9791	- 0.0437

TABLE 1

CONTINUED.

α	$C_{D_{N+C}}$	$(-)\ C_{L_{N+C}}$	C_{D_N}	$(-)\ C_{L_N}$
35	- 0.7427	- 0.0013	0.9766	- 0.0472
36	0.7401	- 0.0018	0.9741	- 0.0508
37	0.7383	- 0.0026	0.9713	- 0.0545
38	0.7367	- 0.0036	0.9686	- 0.0584
39	0.7351	- 0.0049	0.9654	- 0.0623
40	0.7334	- 0.0065	0.9618	- 0.0664
41	0.7313	- 0.0078	0.9576	- 0.0706
42	0.7293	- 0.0094	0.9546	- 0.0748
43	0.7270	- 0.0112	0.9513	- 0.0793
44	0.7247	- 0.0131	0.9465	- 0.0839
45	0.7222	- 0.0154	0.9409	- 0.0884
46	0.7195	- 0.0178	0.9355	- 0.0931
47	0.7166	- 0.0206	0.9308	- 0.0978
48	0.7136	- 0.0235	0.9273	- 0.1026
49	0.7104	- 0.0265	0.9201	- 0.1075
50	0.7071	- 0.0296	0.9146	- 0.1124
51	0.7034	- 0.0327	0.9087	- 0.1173
52	0.6996	- 0.0360	0.9013	- 0.1223
53	0.6955	- 0.0393	0.8947	- 0.1273
54	0.6910	- 0.0427	0.8883	- 0.1324
55	0.6864	- 0.0463	0.8819	- 0.1374
56	0.6811	- 0.0498	0.8732	- 0.1424
57	0.6755	- 0.0535	0.8651	- 0.1475
58	0.6694	- 0.0571	0.8575	- 0.1524
59	0.6608	- 0.0608	0.8499	- 0.1574
60	0.6548	- 0.0644	0.8411	- 0.1624
61	0.6454	- 0.0683	0.8333	- 0.1672
62	0.6361	- 0.0720	0.8235	- 0.1721
63	0.6267	- 0.0758	0.8153	- 0.1768
64	0.6174	- 0.0794	0.8049	- 0.1815
65	0.6081	- 0.0831	0.7966	- 0.1861
66	0.5988	- 0.0867	0.7862	- 0.1906
67	0.5895	- 0.0903	0.7758	- 0.1950
68	0.5801	- 0.0938	0.7653	- 0.1993
69	0.5708	- 0.0973	0.7550	- 0.2034
70	0.5615	- 0.1007	0.7446	- 0.2074
71	0.5522	- 0.1038	0.7343	- 0.2113

TABLE 1

CONCLUDED.

α	$C_{D_N} + C$	$C_{L_N} + C$	C_{D_N}	C_{L_N}
72	0.5428	- 0.1069	0.7216	- 0.2151
73	0.5335	- 0.1099	0.7104	- 0.2186
74	0.5242	- 0.1127	0.6965	- 0.2221
75	0.5149	- 0.1154	0.6852	- 0.2252
76	0.5055	- 0.1181	0.6729	- 0.2284
77	0.4962	- 0.1207	0.6605	- 0.2313
78	0.4869	- 0.1232	0.6479	- 0.2339
79	0.4776	- 0.1256	0.6356	- 0.2365
80	0.4682	- 0.1278	0.6232	- 0.2388
81	0.4589	- 0.1297	0.6110	- 0.2409
82	0.4496	- 0.1314	0.5987	- 0.2428
83	0.4403	- 0.1329	0.5861	- 0.2444
84	0.4310	- 0.1341	0.5733	- 0.2459
85	0.4216	- 0.1352	0.5605	- 0.2472
86	0.4123	- 0.1362	0.5482	- 0.2482
87	0.4030	- 0.1369	0.5359	- 0.2490
88	0.3937	- 0.1374	0.5238	- 0.2495
89	0.3843	- 0.1377	0.5118	- 0.2499
90	0.3750	- 0.1378	0.5000	- 0.2500

TABLE 2

BODY CENTROID AND RADIUS OF GYRATION

CONFIGURATION	BODY	x_o/R_B	k^2
Hemisphere	Solid	5/8	$0.2594\ R_B^2$
	Shell without Base	1/2	$0.4167\ R_B^2$
	Shell with Base	2/3	$0.3911\ R_B^2$
Cone	Solid	3/4	$0.1875\ R_B^2$
	Shell without Base	2/3	$0.5556\ R_B^2$
	Shell with Base	0.805	$0.4561\ R_B^2$
Cone Frustum	Solid	0.6397	$0.2328\ R_B^2$
	Shell without Base	0.527	$0.5846\ R_B^2$
	Shell with Base	0.6977	$0.585\ R_B^2$

TABLE 3

HYPERSONIC STABILITY PARAMETERS

SMALL ANGLE OF ATTACK			
Hemisphere	Solid Body	Shell without Base	Shell with Base
C_{N_α}	1.0000	1.0000	1.0000
C_{N_q}	0.3750	0.5000	0.3333
C_{M_α}	- 0.3750	- 0.5000	- 0.3333
C_{M_q}	- 0.1406	- 0.2500	- 0.1111
Cone			
C_{N_α}	1.0000	1.0000	1.0000
C_{N_q}	0.5833	0.6667	0.5283
C_{M_α}	- 0.5833	- 0.6667	- 0.5283
C_{M_q}	- 0.5625	- 0.6667	- 0.5013
Cone Frustum			
C_{N_α}	1.2361	1.2361	1.2361
C_{N_q}	0.7703	0.8563	0.7260
C_{M_α}	- 0.7703	- 0.8563	- 0.7260
C_{M_q}	- 0.4278	- 0.5560	- 0.3665

TABLE 3

CONTINUED.

45 DEGREE ANGLE OF ATTACK			
Hemisphere	Solid Body	Shell without Base	Shell with Base
C_{N_α}	$2.3918 + 0.3826\ \bar{q}$	$2.3918 + 0.4887\ \bar{q}$	$2.3918 + 0.3472\ \bar{q}$
C_{N_q}	$0.1835 + 0.2206\ \bar{q}$	$0.2865 + 0.2809\ \bar{q}$	$0.1492 + 0.2005\ \bar{q}$
C_{M_α}	$-0.8969 - 0.1434\ \bar{q}$	$-1.1959 - 0.2444\ \bar{q}$	$-0.7972 - 0.1157\ \bar{q}$
C_{M_q}	$-0.0688 - 0.0827\ \bar{q}$	$-0.1433 - 0.1405\ \bar{q}$	$-0.0497 - 0.0668\ \bar{q}$
Cone			
C_{N_α}	2.0000	2.0000	2.0000
C_{N_q}	0.9167	1.0000	0.8617
C_{M_α}	-1.1667	-1.3333	-1.0567
C_{M_q}	0.0208	-0.1111	0.1003
Cone Frustum			
C_{N_α}	$2.9686 + 1.5271\ \bar{q}$	$2.9686 + 1.6379\ \bar{q}$	$2.9686 + 1.4700\ \bar{q}$
C_{N_q}	$1.0734 + 1.7078\ \bar{q}$	$1.1767 + 1.6302\ \bar{q}$	$1.0202 + 1.7478\ \bar{q}$
C_{M_α}	$0.3376 + 0.0973\ \bar{q}$	$0.1310 - 0.0858\ \bar{q}$	$0.4439 + 0.1866\ \bar{q}$
C_{M_q}	$-1.6195 - 0.1206\ \bar{q}$	$-1.6322 - 0.2379\ \bar{q}$	$-1.6158 - 0.0630\ \bar{q}$

TABLE 4

SMALL ANGLE OF ATTACK

Body	STABILITY					
	Hemisphere		Cone		Cone Frustum	
	Static	Dynamic	Static	Dynamic	Static	Dynamic
Solid	(+)	(-)	(+)	(+)*	(+)	(+)*
Shell	(+)*	(-)*	(+)*	(+)	(+)*	(+)
Shell with Base	(+)	(-)	(+)	(+)	(+)	(+)

45 DEGREE ANGLE OF ATTACK

Body	STABILITY					
	Hemisphere		Cone		Cone Frustum	
	Static	Dynamic	Static	Dynamic	Static	Dynamic
Solid	(+)	(-)	(+)	(-)	(-)	(+)*
Shell	(+)*	(-)*	(+)*	(-)*	(-)*	(+)
Shell with Base	(+)	(-)	(+)	(-)	(-)	(+)

NOTE: (+) indicates a stable condition

(-) indicates an unstable condition

* indicates the most stable body condition

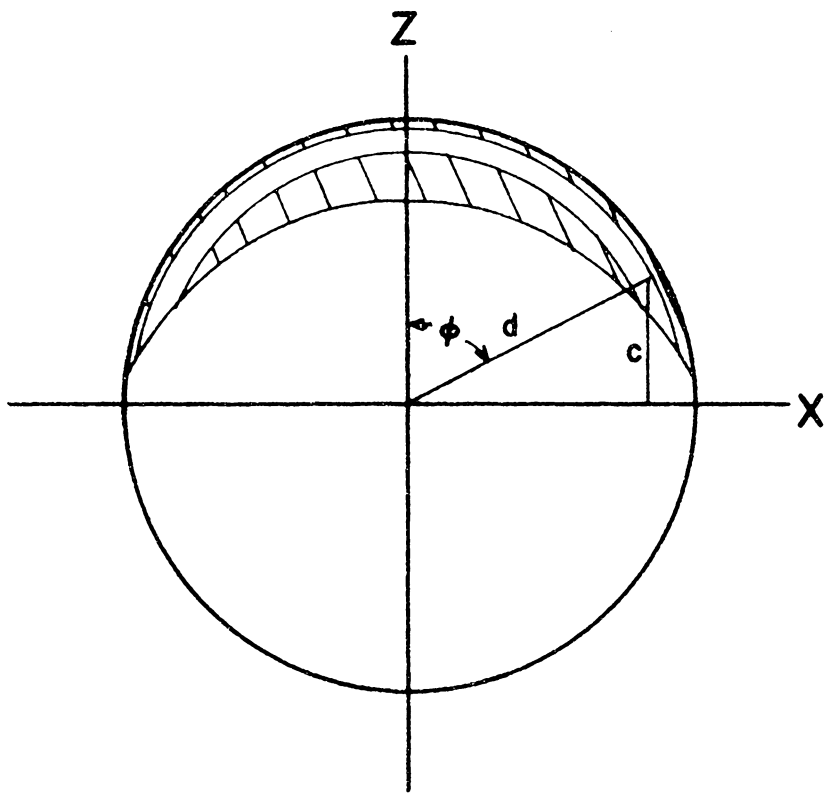

Figure 1

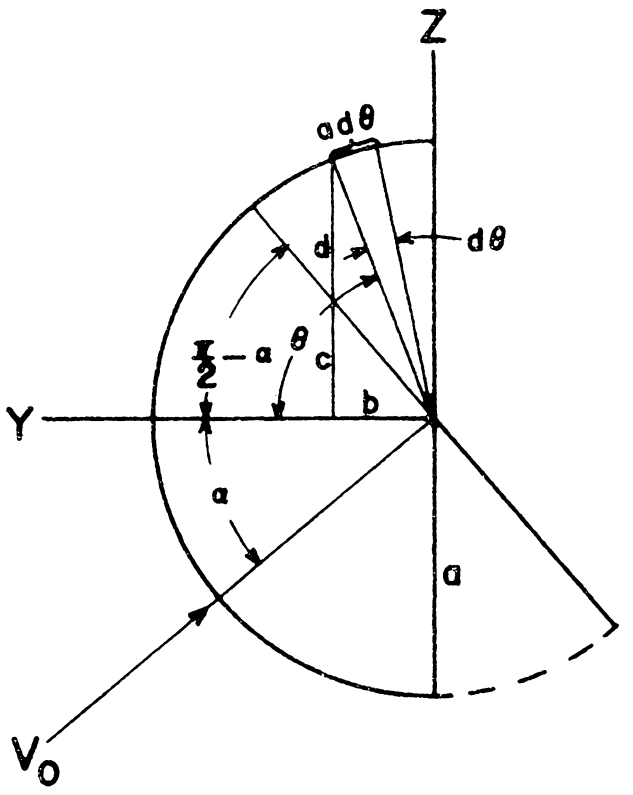

Figure 2

Hemisphere Body Coordinates

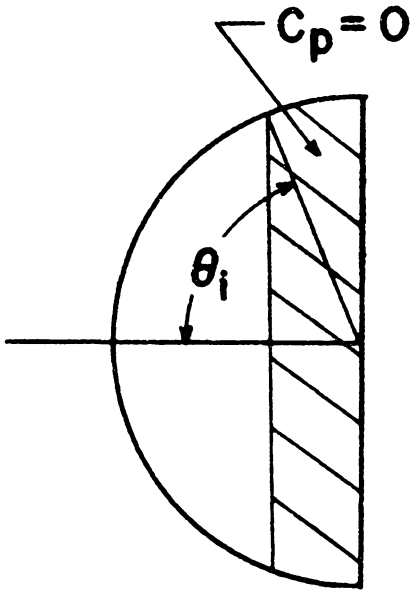

Figure 3

Effect of Centrifugal Forces on the Hemisphere

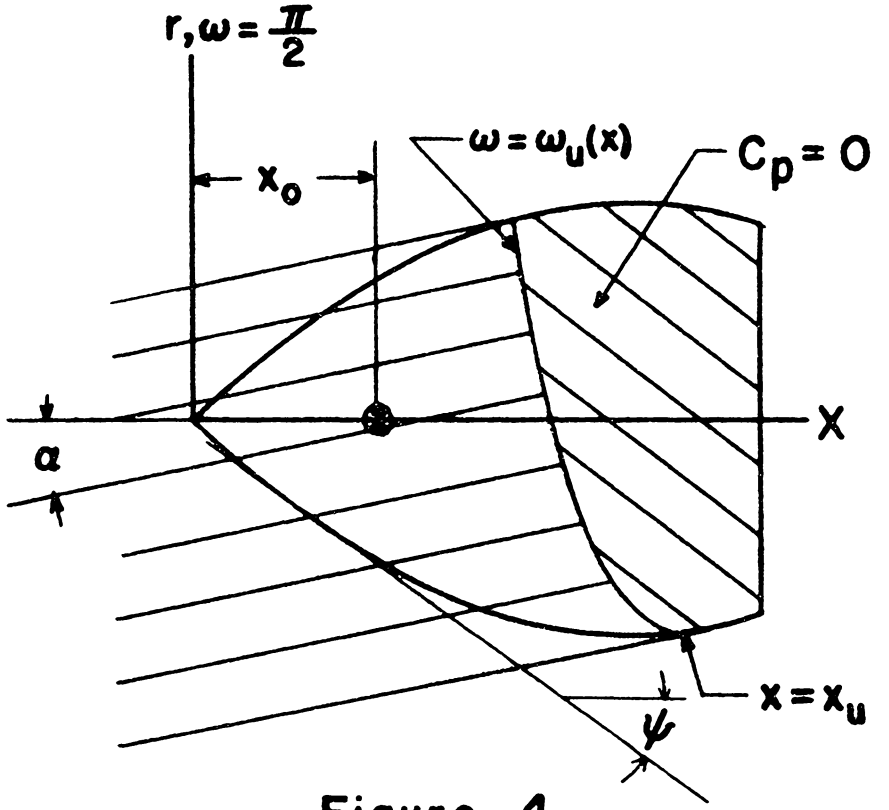

Figure 4

General Body of Revolution (Stability Coordinates)

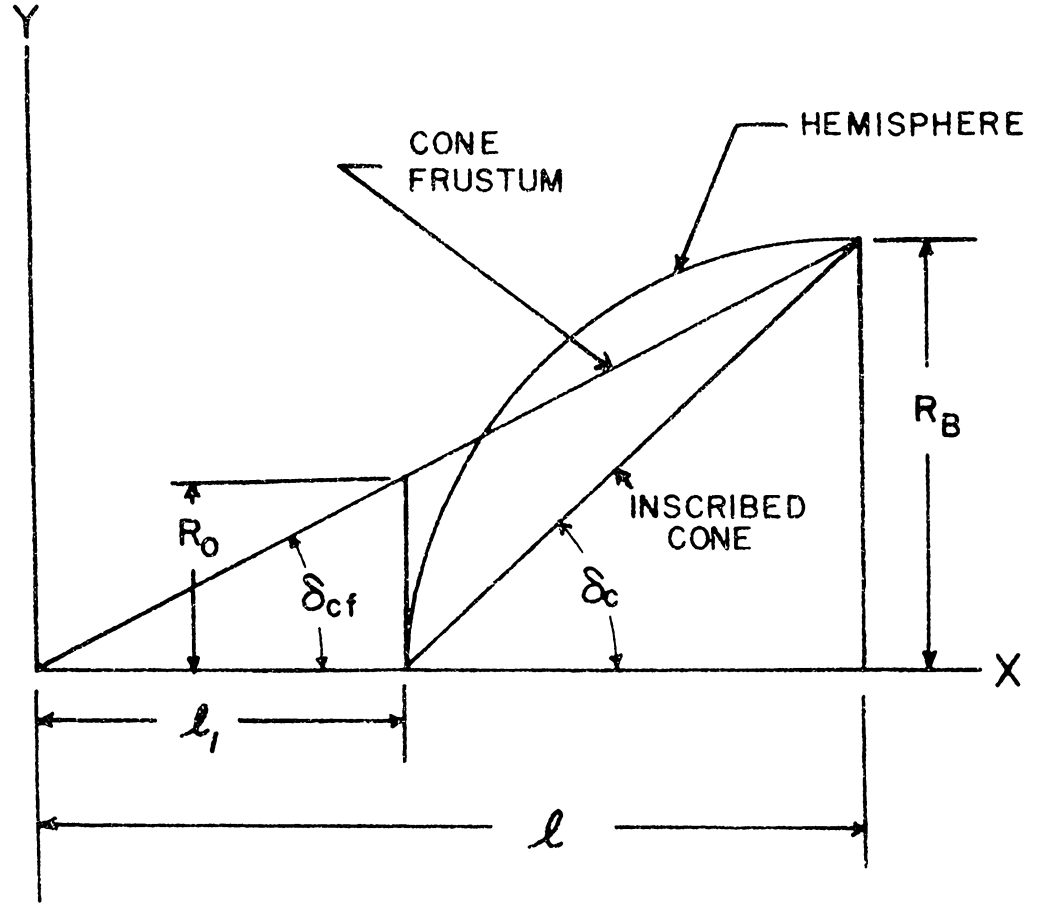

FIGURE 5a

Minimum — Drag Cone Frustum

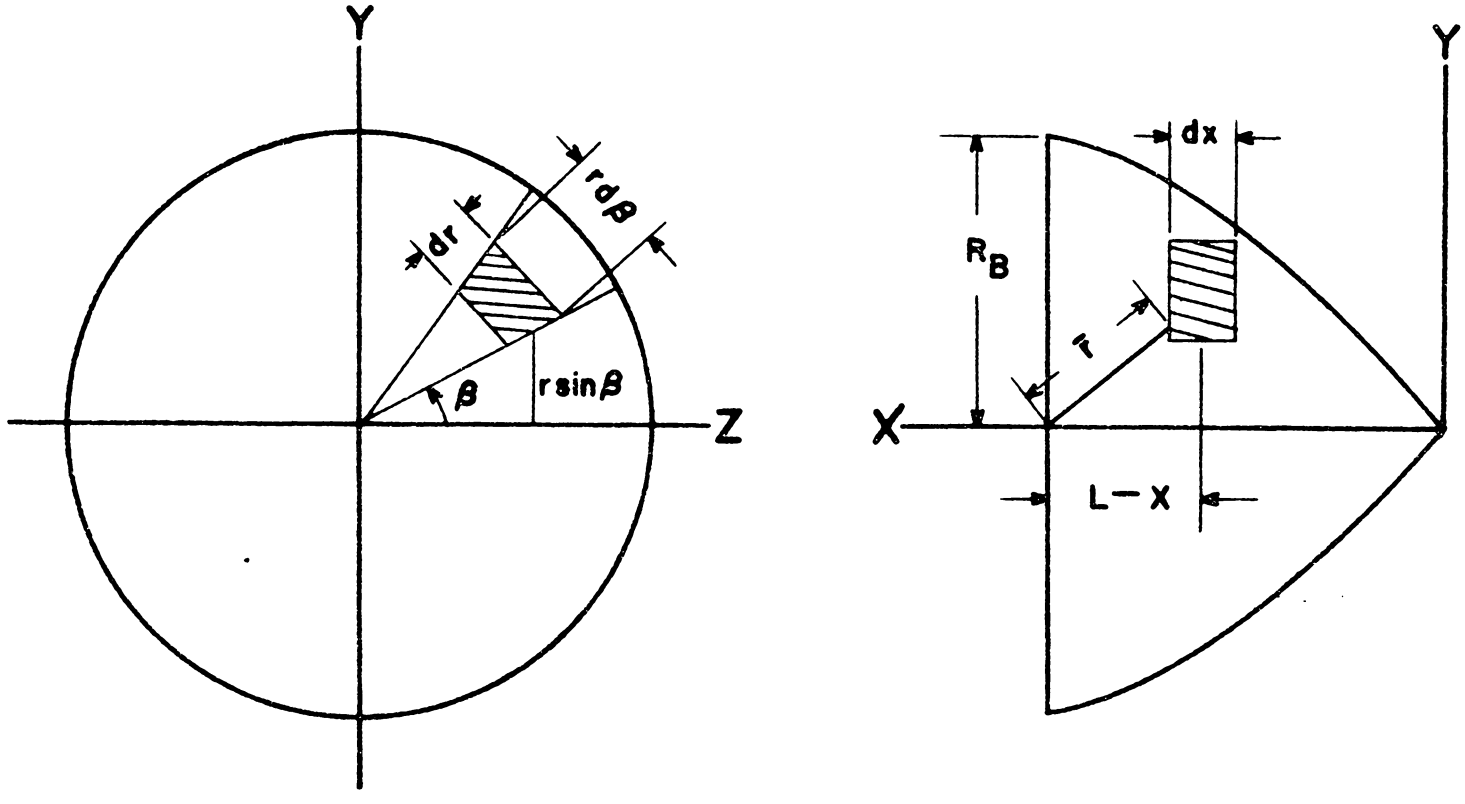

Figure 5b

General Body of Revolution
(Determination of Radius of
Gyration)

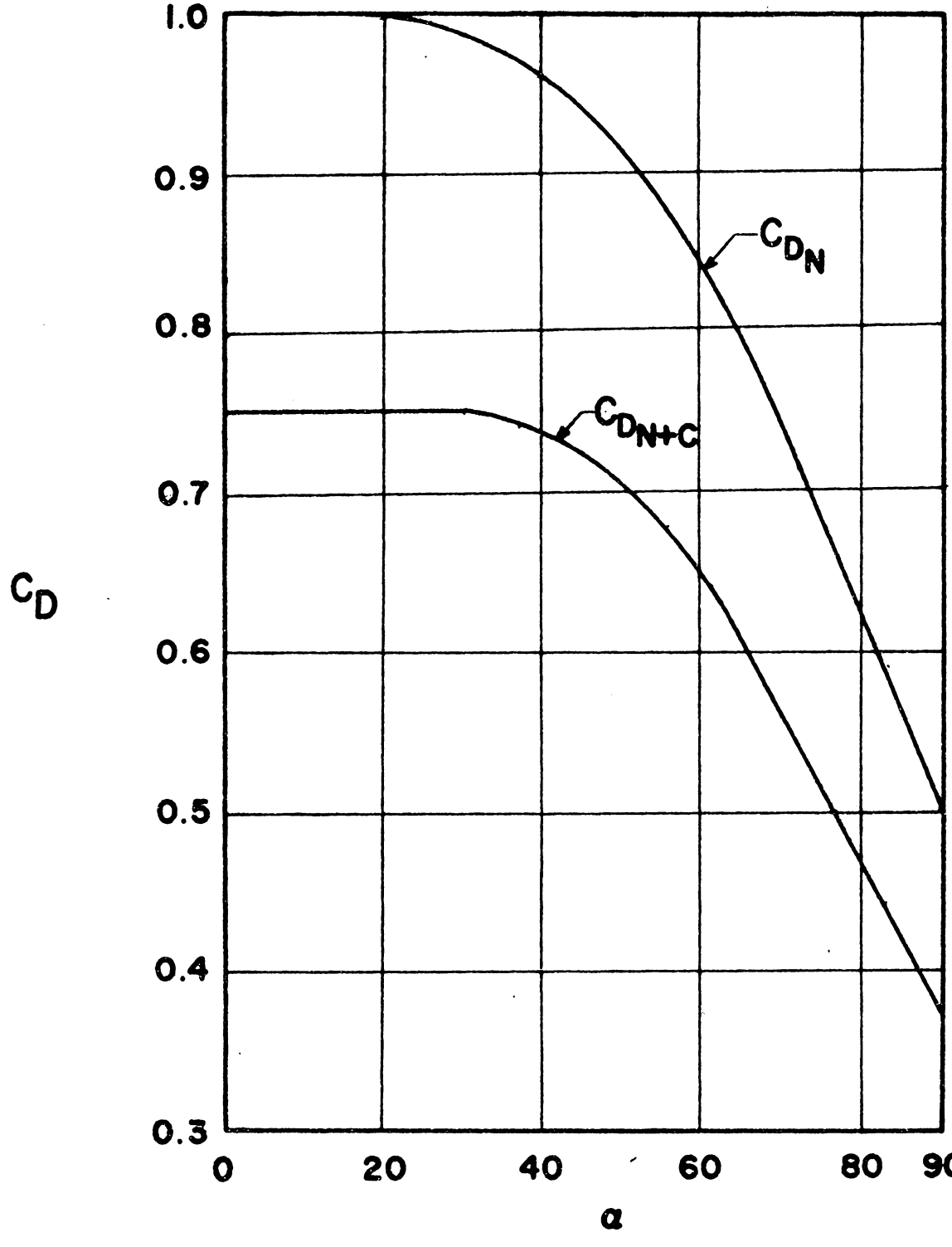

Figure 6

Hemisphere Drag Coefficient

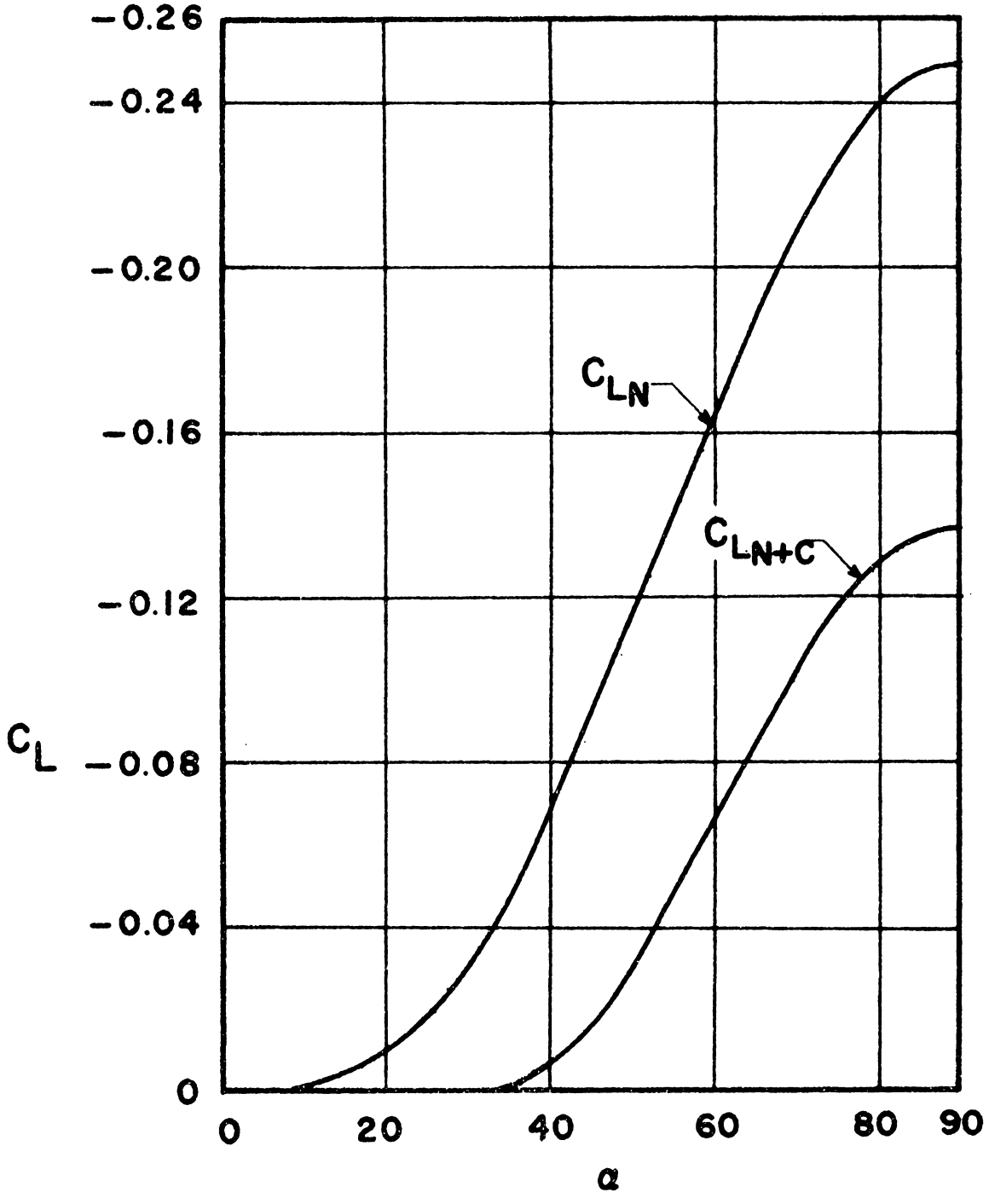

Figure 7

Hemisphere Lift Coefficient

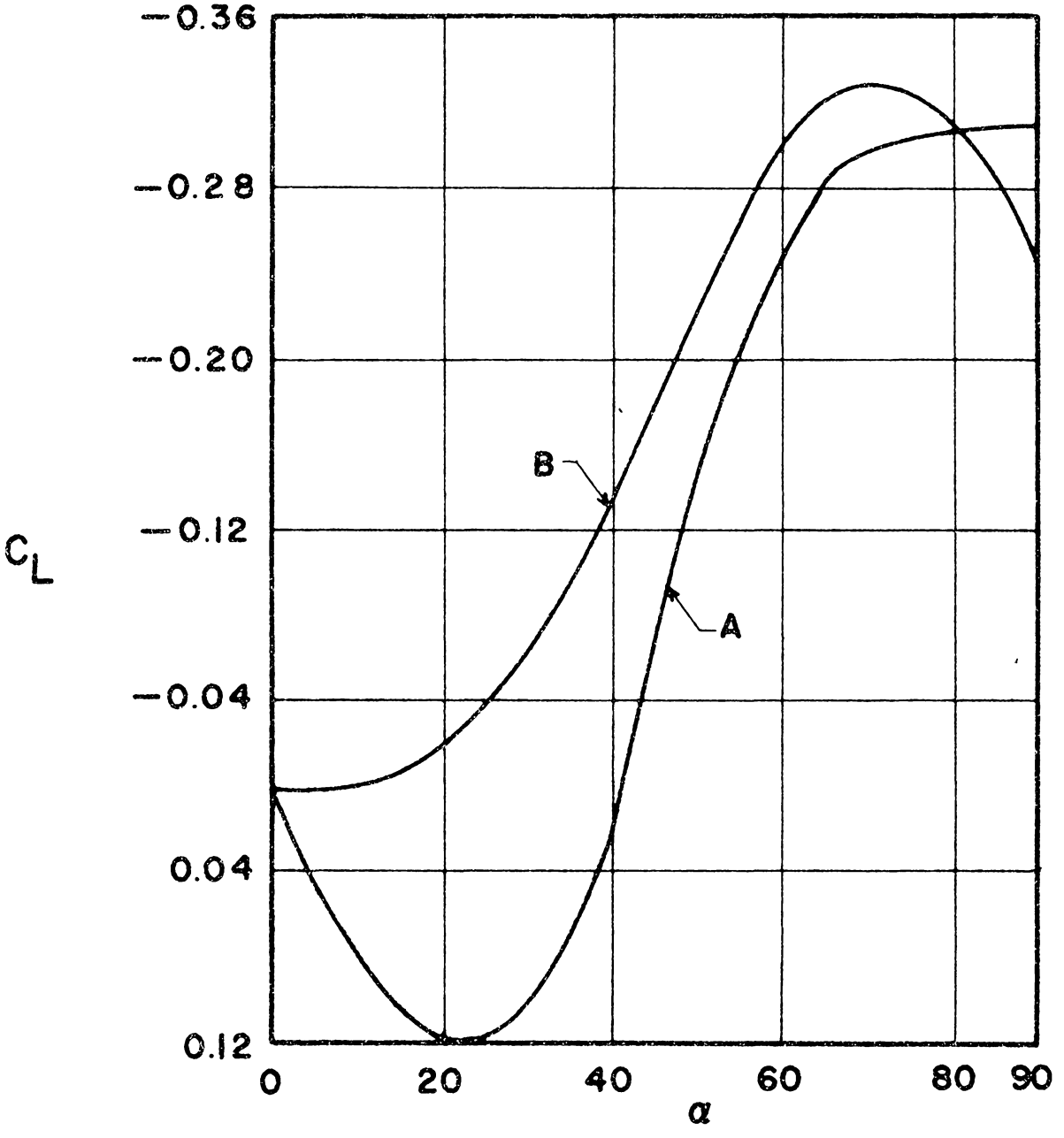

A — Minimum-Drag Cone Frustum

B — Inscribed Cone

Figure 8

Cone and Cone Frustum Lift Coefficient

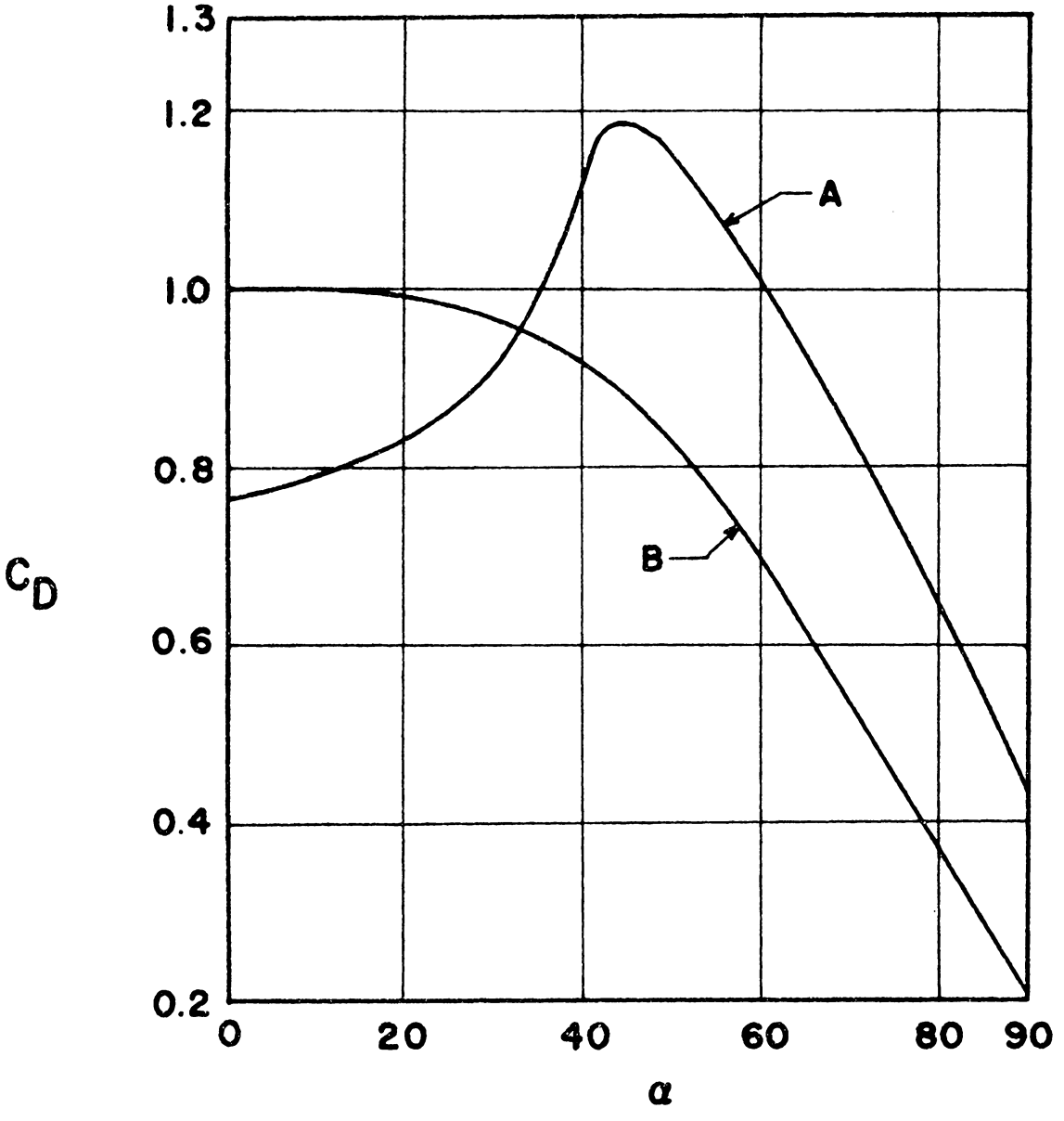

A—Minimum-Drag Cone Frustum
B—Inscribed Cone

Figure 9

Cone and Cone Frustum Drag Coefficient

AERODYNAMIC CHARACTERISTICS OF A HEMISPHERE AT HYPERSONIC SPEEDS

by

Edgar Brian Pritchard

ABSTRACT

It is the purpose of the present thesis to investigate several missile nose configurations to determine the most efficient body from the standpoint of both aerodynamic characteristics and stability. Three configurations were chosen to be studied. These are:

(1) A hemisphere

(2) A cone inscribed in the hemisphere

(3) The minimum-drag cone frustum for the same fineness ratio as the hemisphere.

For each of the above bodies, Newton's impact theory was applied to obtain the lift and drag coefficients for an angle of attack range of zero to 90 degrees.

In addition to the aerodynamic force coefficients, the static and dynamic stability of each of these configurations were studied. In this part of the investigation three physical mass distributions were chosen for each body type; namely,

(1) A solid, homogeneous body

(2) A shell body with no base

(3) A shell body with a base.

In order to investigate the static and dynamic stability it was necessary to define the parameters C_{N_α}, C_{N_q}, C_{M_α}, and C_{M_q}. Having defined the above parameters the stability of each missile nose configuration was obtained for each physical mass distribution.